# TFAP2 paralogs pioneer chromatin access for MITF and directly inhibit genes associated with cell migration

Colin Kenny[1], Ramile Dilshat [2], Hannah Seberg[1+], Eric Van Otterloo[1*], Gregory Bonde[1], Annika Helverson[1], Eiríkur Steingrímsson[2], Robert A. Cornell[1, #]

1. Department of Anatomy and Cell Biology, College of Medicine, University of Iowa, Iowa City, Iowa

2. Department of Biochemistry and Molecular Biology, BioMedical Center, Faculty of Medicine, University of Iceland, Sturlugata 8, 101 Reykjavik, Iceland

[+] Current address: University of Manchester

* Current address: Iowa Institute for Oral Health Research, Department of Anatomy and Cell Biology, Department of Periodontics, College of Dentistry, University of Iowa, Iowa City, Iowa

[#]Corresponding author:

Robert-cornell@uiowa.edu, 319-335-8908

Conflict of interest statement: CK, RD, HS, EVO, GB, AH, ES and RAC declare no conflicts of interest.

Key words: MITF, TFAP2A, TFAP2C, chromatin, nucleosome, pioneer factor, transcriptional activation, repression.

## Abstract

Transcription factors in the Activating-enhancer-binding Protein 2 (TFAP2) family redundantly regulate gene expression in melanocytes and melanoma. Previous ChIP-seq experiments indicate that TFAP2A and Microphthalmia-associated Transcription Factor (MITF), a master regulator in these cell types, co-activate enhancers of genes promoting pigmentation. Evidence that TFAP2 paralogs can serve as pioneer factors supports the possibility that TFAP2 facilitates MITF binding at co-bound enhancers, although this model has not been tested. In addition, while MITF and TFAP2 paralogs both appear to repress genes that promote invasion, whether they do so by co-repressing enhancers is unknown. To address these questions we evaluated gene expression, chromatin accessibility, TFAP2A and MITF binding, and chromatin marks characteristic of active enhancers in SK-MEL-28 melanoma cells that were wild-type or deleted of the two *TFAP2* paralogs with highest expression, *TFAP2A* and *TFAP2C* (i.e., *TFAP2*-KO cells). Integrated analyses revealed distinct subsets of enhancers bound by TFAP2A in WT cells that are inactivated and activated, respectively, in *TFAP2*-KO cells. At enhancers bound by both MITF and TFAP2A, MITF is generally lost in *TFAP2A/TFAP2C* double mutants, but not vice versa, implying TFAP2 pioneers chromatin access for MITF. There is a strong correlation between the sets of genes inhibited by MITF and TFAP2, although we did not find evidence that TFAP2 and MITF inhibit enhancers cooperatively. The findings imply that MITF and TFAP2 paralogs cooperatively affect the melanoma phenotype.

## Introduction

Gene expression in developing melanocytes and melanoma, a cancer derived from the melanocyte lineage, is regulated by transcription factors including Microphthalmia-associated transcription factor (MITF) and members of the SOXE, PAX and TFAP2 families (Atchison, 2014; Betancur et al., 2010; Eckert et al., 2005; Goding, 2000; Hartman and Czyz, 2015; Hoek et al., 2008b; Mollaaghababa and Pavan, 2003; Seberg et al., 2017a; Strub et al., 2011; Van Otterloo et al., 2010; Van Otterloo et al., 2012). MITF is required for differentiation of melanocytes during development, and its activity is regulated at both the transcriptional and post-

translational levels (Rambow et al., 2019). In melanoma cells, high levels of MITF activity promote cell proliferation and pigmentation, while lower levels promote an invasive phenotype (Carreira et al., 2006; Rambow et al., 2019). Mass spectroscopy revealed that MITF interacts with components of both the PBAF chromatin remodeling complex, including BRG1 and CDH7, and the NURF remodeling complex, including RBBP4 (de la Serna et al., 2006; Laurette et al., 2015). Furthermore, chromatin immunoprecipitation of BRG1 in cells depleted of *MITF* revealed that MITF recruits BRG1 to the promoters of specific genes, including *TYR*, which encodes the rate-limiting enzyme in melanin synthesis Tyrosinase (Laurette et al., 2015). Similar analysis suggested that SOX10 also recruits BRG1 to chromatin, and at some loci it does so in co-operation with MITF (Laurette et al., 2015). Conversely, there is evidence that PAX3 inhibits the activity of MITF at the *DCT* promoter (Lang et al., 2005). Furthermore, low MITF activity is associated with an invasive phenotype, and deletion or knockdown of *MITF* results in upregulation of genes that promote migration and invasion (Dilshat et al., 2021). MITF CUT&RUN peaks are found near some genes whose expression is upregulated in *MITF* mutant cells, implying MITF directly represses their expression (Dilshat et al., 2021).This set of MITF peaks is enriched for the binding site of FOXC1, a transcriptional repressor (Du et al., 2012), suggesting MITF has co-factors in its repressive function as well as its activating one.

The activating enhancer-binding family of transcription factors, comprising five members, TFAP2A-E, regulate development of many cell types and organs including neural crest, placodes, epidermis, trophectoderm, heart, kidney, and brain (Bamforth et al., 2001; Brewer et al., 2002; Knight et al., 2003; Kuckenberg et al., 2012; Luo et al., 2002; Mitchell et al., 1991; Moser et al., 1997; Schorle et al., 1996; Tan et al., 2008; Wang et al., 2006). In several contexts, including melanocyte differentiation, TFAP2 paralogs function redundantly (Kołat et al., 2021; Li and Cornell, 2007; Van Otterloo et al., 2010; Wang et al., 2008). For instance, in zebrafish *tfap2a* loss-of-function mutant embryos the number of melanocytes is lower than normal and pigmentation is profoundly delayed relative to in wild type embryos; this phenotype is exacerbated if *tfap2a* mutant embryos are also depleted of *tfap2e* expression with antisense morpholinos (Van Otterloo et al., 2010). In zebrafish melanoma Tfap2a and Tfap2e also appear to act redundantly to promote proliferation and, interestingly,

88 to suppress cell adhesion and cell migration (Campbell et al., 2021). Consistent with
89 redundant function of Tfap2 paralogs in the melanocyte lineage, in the skin of mouse
90 embryos with neural-crest specific knockout of the two paralogs with highest
91 expression, *Tfap2a* and *Tfap2b*, there are fewer-than-normal cells expressing
92 markers of melanocytes (Seberg et al., 2017b).
93
94 Tfap2 paralogs and MITF appear to co-activate certain genes. For instance, in a
95 human melanoma cell line, the *in vitro* enhancer activity of an element within an *IRF4*
96 intron depended on the simultaneous binding of MITF and TFAP2 (Praetorius et al.,
97 2013). Further, in zebrafish *tfap2a* and *mitfa* double mutant embryos there is a
98 greater-than-additive reduction in the number, and level of pigmentation, of
99 melanocytes in comparison to in single mutants (Seberg et al., 2017b). Evidence that
100 Tfap2 paralogs and Mitfa operated in parallel, rather than Tfap2 paralogs functioning
101 upstream of *mitfa* expression, is that in *tfap2a/tfap2e* doubly-depleted zebrafish
102 embryos, *mitfa* expression, and the number of *mitfa*-expressing cells, are not
103 significantly changed from *tfap2a* singly depleted embryos (Seberg et al., 2017b).
104 Supporting parallel activity of Tfap2 paralogs and MITF, the promoters of MITF target
105 genes are enriched for TFAP2 consensus binding sites (Laurette et al., 2015;
106 Rambow et al., 2015). Moreover, ChIP-seq experiments in primary melanocytes
107 suggest that TFAP2A and MITF bind overlapping regions of chromatin near genes
108 encoding regulators of pigmentation (Seberg et al., 2017b). Collectively, these
109 observations indicate that TFAP2 paralogs co-activate a subset of MITF target genes
110 by binding at the same enhancers. Still unclear, however, is whether they also co-
111 repress enhancers, and whether TFAP2 paralogs and MITF act cooperatively or
112 independently at enhancers they co-regulate.

113 TFAP2 paralogs may serve as pioneer factors for MITF, although not all evidence
114 supports this possibility. *Pioneer* or *initiating* TFs can bind nucleosome-bound DNA
115 and recruit other TFs that lack this property called *settler TFs* (reviewed in Voss and
116 Hager, 2014; Zaret, 2020; Zaret and Carroll, 2011). Evidence that TFAP2 paralogs
117 are pioneer factors includes, first, that TFAP2 binding site is over-represented within
118 DNase1-protected “footprints” in mouse embryonic stem cells induced to differentiate
119 (Sherwood et al., 2014). Second, TFAP2A catalyzes assisted loading of androgen
120 receptor (AR) in epididymis cells (Pihlajamaa et al., 2014) and estrogen receptor in

121 MCF-7 cells (Tan et al., 2011). Third, the TFAP2 binding site is enriched for at the
122 center of ATAC-seq peaks, implying it has a strong effect on chromatin accessibility
123 (Grossman et al., 2018). Fourth, ATAC-seq peaks in naïve-stated human ESC
124 showed reduced openness in TFAP2C KO cells (Pastor et al., 2018), and forcing
125 expression of TFAP2C in human ESC is sufficient to open chromatin at loci where it
126 binds (Li et al., 2019). Finally, TFAP2A, TFAP2B and TFAP2C can bind
127 nucleosomes (Fernandez Garcia et al., 2019). Together these findings support the
128 possibility that TFAP2 displaces nucleosomes and thereby facilitates chromatin
129 binding by MITF. However, it not clear that MITF needs a pioneer factor to bind
130 chromatin. In the *dynamic-assisted-loading model*, all classes of TFs have short
131 residency on chromatin (reviewed in Voss and Hager, 2014). *Initiating TFs* are able
132 to recruit ATP-dependent chromatin remodelers (nBAF, SWI/SNF, INO80, ISWI,
133 NURD) and thereby make chromatin accessible to other TFs, i.e., the *assisted* TFs
134 (Swinstead et al., 2016b). As mentioned above, MITF binds various components of
135 the SWI/SNF complex (Aras et al., 2019; de la Serna et al., 2006; Keenen et al.,
136 2010) and the chromatin remodeler CHD7 (Laurette et al., 2015) and so meets the
137 criteria for an initiating factor. If the dynamic-assisted-loading model holds in this
138 situation, MITF would have no need for a pioneer factor like TFAP2 to assist its
139 binding to chromatin.

140 To address these questions, we systematically tested the effect of loss of TFAP2
141 paralogs on: nucleosome positioning, using the assay for transposase-accessible
142 chromatin using sequencing (ATAC-seq) methodology; enhancer activity, using
143 cleavage under targets and release using nuclease (CUT&RUN) with anti-H3K27Ac,
144 anti-H3K4me3, and anti-H3K27me3; and binding of MITF, using CUT&RUN. We
145 similarly assessed binding of TFAP2A in cells harboring loss of function mutations in
146 *MITF*. Our results support the notion that TFAP2 factors behave like the canonical
147 pioneer factor FOXA1: at many chromatin elements bound by TFAP2A, loss TFAP2
148 led to loss of enhancer activity, and in a large subset, it also let to chromatin
149 becoming condensed. In both of these subsets of TFAP2-activated enhancers, MITF
150 binding was TFAP2 dependent. In addition, we find evidence that TFAP2 paralogs
151 can also inhibit enhancers, and at a subset of those that they inhibit, they exclude
152 binding of MITF. Finally, the analyses suggest TFAP2 directly inhibits many of the
153 same genes that MITF inhibits, but we do not find evidence that TFAP2 and MITF

154 co-repress the same enhancers. Together these findings illuminate the mechanisms
155 by which TFAP2 and MITF coordinately regulate differentiation of melanocytes and
156 the phenotype of melanoma cells.

157 **Results**

158 **Tfap2a and Tfap2e redundantly promote the differentiation of zebrafish**
159 **embryonic melanocytes**

160 We first sought to use a zebrafish mutant to confirm an earlier conclusion based on
161 morpholino-mediated knockdown that Tfap2 paralogs redundantly promote
162 differentiation of embryonic melanophores. In the melanocyte lineage of zebrafish
163 embryos, levels of *tfap2e* expression are high, those of *tfap2a* and *tfap2c* are lower
164 (~30% of the level of *tfap2e*), and those of *tfap2b* are negligible (Higdon et al., 2013).
165 We previously reported that wild-type (WT) embryos injected with antisense
166 morpholino oligonucleotides (MO) targeting the splicing of *tfap2e* exhibit no overt
167 phenotype, but embryos homozygous for a *tfap2a* loss-of-function allele (i.e., lockjaw
168 , Knight et al., 2003), injected with the *tfap2e* MO have fewer embryonic melanocytes
169 than counterparts injected with a non-targeting control MO, and pigmentation is
170 delayed in them, although it occurs eventually (Van Otterloo et al., 2010). To confirm
171 that the recovery of pigmentation did not simply reflect the transient effects of the
172 *tfap2e* morpholino we used zinc-finger nucleases to engineer zebrafish lines
173 harboring frame-shift-inducing mutations in *tfap2e* (details in **Supplemental Fig.**
174 **S1A-B)**. qPCR analysis showed that expression of the *tfap2e* transcript was
175 significantly lower in *tfap2e* mutant than in WT embryos, suggesting nonsense-
176 mediated decay (**Supplemental Fig. S1C**)**.** As in embryos injected with *tfap2e* MO,
177 there was no overt phenotype in homozygous *tfap2e* mutants (**Supplemental Fig.**
178 **S1D-F**). However, in *tfap2a*/*tfap2e* double mutants the number of melanocytes was
179 significantly reduced in the dorsal stripe at 29 hours post fertilization (hpf) relative to
180 those in *tfap2a* single mutants. At this stage these cells were under-pigmented
181 relative to in non-mutant siblings, although their pigmentation reached wild-type
182 levels by 48 hpf (**Fig. 1A-E; Supplemental Fig. S1G-J**). In summary, the reduction
183 in melanocyte number and delay in pigmentation in *tfap2a/tfap2e* double mutant
184 versus WT embryos implies that TFAP2 paralogs promote melanocyte proliferation
185 and differentiation in a redundant fashion.

186

187 **TFAP2A binds open and closed chromatin**

188 We next sought to learn TFAP2 paralogs interact with MITF in activating and
189 repressing gene expression in a single cell line. We have reported the genes
190 differentially expressed between SK-MEL-28 melanoma cells that are WT or
191 harboring loss-of-function mutations in all alleles of MITF, as well as binding of MITF
192 using cleavage under targets and release under nuclease (CUT&RUN) (Dilshat et
193 al., 2021). Here, again using SK-MEL-28 melanoma cells, we carried out (1)
194 CUT&RUN using antibodies to TFAP2A (i.e., TFAP2A peaks), (2) CUT&RUN using
195 antibodies to chromatin marks indicative of active regulatory elements (H3K27Ac
196 and H3K4Me3) (Creyghton et al., 2010; Pekowska et al., 2011), and of inactive
197 chromatin (H3K27Me3) (Ringrose and Paro, 2004), and (3) ATAC-seq to distinguish
198 between open and closed chromatin (Buenrostro et al., 2013). We used IgG as a
199 background control and the MACS2 software to call peaks in each dataset
200 (**Supplemental Fig. S2A-B**). Based on proximity to transcriptional start sites (TSS),
201 about one-third of TFAP2A peaks appeared to be at or near promoters (within 3 kb
202 of a TSS). As expected, these elements had strong H3K4Me3 signal (**Supplemental**
203 **Fig. S2B**). At promoter-proximal TFAP2A peaks, the H3K27Ac signal in WT cells
204 was relatively consistent, whereas at promoter-distal TFAP2A peaks the H3K27Ac
205 signal ranged from high to background level (**Supplemental Fig. S2B-C**). About two-
206 thirds of TFAP2A peaks overlapped ATAC-seq peaks, indicating that they were in
207 open chromatin (**Supplemental Fig. S2D-E**). Of note, the read depth (height) of a
208 peak approximates the number of chromosome molecules where TFAP2A binds.
209 The average read depth of the TFAP2A peaks in closed chromatin was only about
210 50% of that in open chromatin but was nonetheless 80-fold higher than the IgG
211 background read depth (**Supplemental Fig. S2D-E, Supplemental Fig. S3A-B for**
212 **example loci**). Importantly, the TFAP2 binding site was strongly enriched for in both
213 TFAP2A-bound elements where the local ATAC-seq signal was called as a peak and
214 in counterparts where it was not ($p < 1 \times 10^{-1785}$ and $p < 1 \times 10^{-4375}$, respectively),
215 supporting the idea that TFAP2A binds DNA directly even when the DNA is occupied
216 by nucleosomes (**Supplemental Fig. S3C-D**). These results indicate that TFAP2A

217 binds at both open and closed chromatin, consistent with it being a pioneer factor,
218 and at enhancers and promoters with a range of activity levels.

219

220 **TFAP2A activates enhancers as in pioneer factor and non-pioneer factor**
221 **modes**

222 We next sought to identify enhancers and promoters that TFAP2 paralogs regulate
223 directly, and, of these, the fraction that they regulate as pioneer factors. To these
224 ends we used Crispr/Cas9 methods to introduce frame-shift mutations into the
225 *TFAP2* genes with high expression in SK-MEL-28 cells, *TFAP2A* and *TFAP2C;* we
226 then carried out RNA-seq, ATAC-seq, and CUT&RUN with antibodies to H3K27Ac,
227 H3K4me3, and H3K27me3. In two independent knockout clones (hereafter, *TFAP2*-
228 KO cells), Western blot analysis showed an absence of immunoreactivity for both
229 proteins (**Supplemental Fig. S4A-E**). Control clones (hereafter WT cells) were
230 derived from the parental SK-MEL-28 line transiently transfected with Cas9 but not
231 with guide RNAs. RNA-seq revealed that expression of 532 genes was
232 downregulated, and expression of 609 genes was upregulated, in *TFAP2*-KO cells
233 (i.e., in both clones) versus in WT cells (**Supplemental Fig. S5A volcano plot**). We
234 will refer to these sets as “TFAP2-activated genes” and “TFAP2-inhibited genes,”
235 respectively.

236 To identify candidates for enhancers directly activated by TFAP2 paralogs we first
237 filtered TFAP2A peaks for those in chromatin that was open and active in WT cells
238 (i.e., coinciding with peaks of ATAC-seq and H3K27Ac) (21,745/ 36,948 of TFAP2A
239 peaks), then for those greater than 1 kb from a transcription start site (i.e., to filter out
240 promoters) (11,005/ 21,745), and finally for those where the local H3K27Ac signal
241 was significantly lower (adj $p < 0.05$, log2FC <-1) in *TFAP2*-KO cells relative to in
242 WT cells (3,858/11,005).

243 To determine how often TFAP2 activates enhancers as a pioneer factor, at each
244 directly TFAP2-activated enhancer we evaluated the ATAC-seq signal in WT and
245 TFAP2-KO cells. At about half of the enhancers the ATAC-seq signal was also
246 significantly lower (adj $p < 0.05$, log2FC <-1) in *TFAP2*-KO versus in WT cells (i.e.,

247 the ATAC-seq signal was TFAP2-activated) (**Fig. 2A, E-E'**); at this subset we infer
248 that TFAP2 paralogs function as pioneer factors. At the remaining half, the ATAC-
249 seq signal was unchanged between *TFAP2*-KO versus WT cells (i.e., the ATAC-seq
250 signal was TFAP2-independent) (**Fig. 2B, F-F'**); at this subset we infer that TFAP2
251 paralogs do not function as pioneer factors but rather as a transcriptional activator.
252 Consistent with both subsets indeed being enhancers activated by TFAP2, both
253 were associated with TFAP2-activated genes. Interestingly, the association was
254 stronger for those where TFAP2 functions as a pioneer factor (**Fig. 2 I, J**) (**Table 1**
255 **and Table 2**). Moreover, at both subsets the H3K4me3 signal, which is associated
256 with enhancer activity (Pekowska et al., 2011), was reduced in *TFAP2*-KO cells
257 relative to in WT cells (**Fig. 2E'', F''**). While both subsets were strongly enriched for
258 the TFAP2 binding site and certain other binding sites (e.g., RUNX), the subset
259 pioneered by TFAP2 was more strongly enriched for the SOXE and MITF binding
260 sites, while the non-pioneered subset was more strongly enriched for the FRA1,
261 TEAD and the ZFX binding sites (**Fig. 2M, N**). Of note, FRA1 is a pioneer factor (Lee
262 et al., 2018) which could explain why these elements do not depend on TFAP2 to be
263 free of nucleosomes.

264

265 **TFAP2A inhibits enhancers by blocking the opening of chromatin**

266 Because of evidence that TFAP2A directly represses gene expression (Lin et al.,
267 2016; Liu et al., 2007; Wong et al., 2012) we next sought to identify candidates for
268 enhancers directly inhibited by TFAP2 paralogs. To this end we filtered promoter-
269 distal TFAP2A peaks for those where the local H3K27Ac signal was higher in
270 *TFAP2*-KO cells than in WT cells (adj. $p < 0.05$, $\log2FC > 1$). Analogously to TFAP2-
271 activated enhancers, candidate TFAP2-inhibited enhancers were split between a
272 subset where the ATAC-seq signal was higher in *TFAP2*-KO cells than in WT cells
273 (i.e., TFAP2-inhibited) (**Fig. 2C, G-G'**) and a subset where it was TFAP2-
274 independent (**Fig. 3D, H-H'**). The first subset was significantly associated with
275 TFAP2-inhibited genes (**Fig. 3K**, **Table 1 and Table 3**) and the average H3K4me3
276 signal at these sites was TFAP2-inhibited (**Fig. 3G''**). Because TFAP2 concomitantly
277 inhibits enhancer activity and chromatin accessibility, we define these enhancers as

278 inhibited by TFAP2 in pioneer factor-mode. The binding site for TFAP2 site was
279 strongly enriched for in these sites, as were those for ETS1 and CTCF (**Fig. 3O**),
280 both transcriptional repressors (Kim et al., 2015; Mavrothalassitis and Ghysdael,
281 2000). By contrast, the subset of candidate TFAP2-inhibited enhancers where the
282 ATAC-signal was TFAP2-independent was not associated with TFAP2-inhibited
283 genes (**Fig. 3L**, **Table 1**), and the average H3K4me3 signal at them was TFAP2
284 independent (**Fig. 3H''**). We infer these elements are not TFAP2-inhibited
285 enhancers, despite having elevated H3K27Ac signal in TFAP2-KO cells in
286 comparison to WT cells. In conclusion, at TFAP2-inhibited enhancers TFAP2
287 recruits machinery that condenses chromatin and inhibits enhancer activity; the
288 canonical pioneer factor FOXA1 also has this potential (Sekiya and Zaret, 2007;
289 Watts et al., 2011).

290 We similarly analyzed whether and how TFAP2 directly activates or directly inhibits
291 promoters. Although TFAP2A peaks are frequently found at promoters (8277 genes
292 have a TFAP2A peak within 1 kb of the TSS), it was uncommon for the underlying
293 H3K27Ac and H3K4Me3 signal to be elevated or reduced in *TFAP2* KO cells relative
294 to in WT cells (119 and 31 candidate for directly activated and directly inhibited
295 promoters, respectively). Similar to the trends for TFAP2-regulated enhancers, the
296 pioneered subset of TFAP2-activated promoters was more strongly associated with
297 TFAP2-activated genes than the non-pioneered subset, and only the pioneered
298 subset of TFAP2-inhibited promoters was associated with TFAP2-inhibited genes
299 (**Supplemental Fig. S6A-L; additional examples in Supplemental Fig. S7A-B**).

300

301 **At additional subsets of MITF peaks overlapping TFAP2A peaks, TFAP2**
302 **facilitates chromatin access for MITF both in pioneer and non-pioneer factor**
303 **modes**

304 A prediction of the TFAP2-as-pioneer-factor model is that binding of transcription
305 factors, like MITF, will depend on TFAP2. Among 37,643 MITF peaks in WT SK-
306 MEL-28 cells that we previously identified by CUT&RUN (Dilshat et al., 2021),
307 15,752 (42%) overlap a TFAP2A peak (i.e., assessed in this study). Of these, 9,413
308 (60%) were within open and active chromatin (**Supplemental Fig. S8A**). To assess

309 MITF binding in the absence of TFAP2 we carried out anti-MITF CUT&RUN in
310 *TFAP2*-KO cell lines. Of note, as *MITF* RNA levels in *TFAP2*-KO cells are only about
311 60% of those in WT cells, an across the board decrease in the average height (read
312 depth) of MITF peaks was possible. Instead we observed that the average height of
313 MITF peaks not overlapping TFAP2A peaks was equivalent in *TFAP2*-KO cells and
314 in WT (**Supplemental Fig. S8B**). By contrast, among MITF peaks overlapping
315 TFAP2A peaks (15,752), the height of 5,443 (35%) was significantly lower in *TFAP2*-
316 KO cells than in WT cells (adj. p <0.05, log2FC < -1). (**Fig. 3A-D; Supplemental**
317 **Fig. S8C-D and Supplemental Fig. S9**). We refer to these as "TFAP2-dependent
318 MITF peaks," referring only to MITF peaks that appear to be directly TFAP2-
319 dependent (because they overlap TFAP2A peaks in WT cells).

320

321 We reasoned that TFAP2 paralogs could facilitate MITF binding by displacing
322 nucleosomes (i.e., in pioneer factor mode) or alternatively by elevating MITF's affinity
323 for open DNA. Consistent with both models, we observed that TFAP2-dependent
324 MITF peaks were in three subsets with respect to the TFAP2-dependence of the
325 underlying ATAC-seq signal. At about 57% (3,083/5,443) the ATAC-seq signal was
326 significantly lower (**Fig. 3B-C, 3F-F'**), at 37% (2,022/5,443) it was unchanged (**Fig.**
327 **3D, 3G-G'**), and at 6% it was higher (**Fig. 3E, 3H-H'**) in *TFAP2*-KO cells than in WT
328 cells. The first two subsets were strongly associated with TFAP2-activated genes
329 (Hypergeometric test; p-value = $8.4 \times 10^{-26}$ and p-value = $1.07 \times 10^{-13}$ respectively)
330 and with MITF-activated genes (Hypergeometric test; p-value = $1.16 \times 10^{-21}$ and p-
331 value = $4.3 \times 10^{-11}$ respectively) **(Table 4)**. We infer that at the first subset, TFAP2 is
332 a pioneer factor, facilitating access for MITF and other transcription factors
333 (illustrated in **Fig. 3F''**). Supporting this prediction, the transcription factor binding
334 sites for MITF, SOX10, RUNX and FRA1 were strong enriched at such elements
335 (**Fig. 3F'''**). At the second subset, TFAP2 is a transcriptional activator that recruits
336 MITF, also functioning as a transcriptional activator; we presume another protein
337 serves as a pioneer factor at this subset (illustrated in **Fig. 3G''**). Consistent with this
338 notion, the binding site for JUN, a widely deployed pioneer factor (Vierbuchen et al.,
339 2017), site is strongly enriched in these elements (**Fig. 3G'''**). Examples are shown
340 of TFAP2-dependent MITF peaks near *FRMD4B, CYP7B1, TRPM1 SOX9, EDNRB,*
341 *MREG, GPR143, SNAI2, MEF2C, MYO5A, PAX3, EN1* and *FOXI3* genes (**Fig. 3B-D**

342 **and Supplemental Fig. S8D**). At the third subset of TFAP2-dependent MITF peaks,
343 where ATAC-seq signal was higher in *TFAP2*-KO cells than in WT cells
344 (**Supplemental Fig. S10A-A'**), TFAP2 may serve as a pioneer factor for MITF in
345 MITF's proposed role as transcriptional repressor (Dilshat et al., 2021) (**illustrated in**
346 **Supplemental Fig. S10A''**). However, this category of element was not enriched
347 near genes inhibited by either TFAP2 or MITF (Hypergeometric test; p-value = 6.02 x
348 $10^{-02}$ and p-value = 9.12 x $10^{-02}$ respectively). These results are consistent with
349 TFAP2 facilitating access for MITF, in its transcriptional activator form, to enhancers
350 in both pioneer-factor and non-pioneer factor modes.

351 To test for the converse dependence, we carried out anti-TFAP2A CUT&RUN in
352 *MITF*-KO cells. *TFAP2A* mRNA levels were equivalent in *MITF*-KO and WT cells,
353 and the average TFAP2A peak height was globally equivalent by CUT&RUN. At 13%
354 (717/ 5334) of TFAP2-dependent MITF peaks, the TFAP2A peak was, reciprocally,
355 significantly reduced in *MITF*-KO cells (**Fig. 3A, C**). At such loci, the average ATAC-
356 seq was reduced in *TFAP2*-KO cells than in WT cells (**Fig. 3C, 3I-I'**). We termed
357 these peaks mutually-dependent (**illustrated in Fig. 3I''**)**.** Interestingly, mutually-
358 dependent MITF/ TFAP2 peaks were enriched in binding motifs for TFAP2, MITF,
359 BRM2 and TEAD4 but, notably and unlike the other subsets of TFAP2-dependent
360 MITF peaks, not for SOXE (**Fig. 3I'''**)**.** SOX10 co-binds many loci with MITF
361 (Laurette et al., 2015), if SOX10 is absent from mutually-dependent peaks this may
362 explain the dependence of TFAP2 binding on MITF at these sites. At ~40% (288/
363 717) of the mutually dependent peaks, the polycomb repressive histone mark
364 H3K27Me3 was significantly higher (including in the gene body) in *MITF*-KO cells
365 but, unexpectedly, not in *TFAP2*-KO cells, even though MITF binding was lower in
366 *TFAP2*-KO cells **(illustrated in Fig 3I'', Supplemental Fig. 8E-G**).

367 In summary, at about one third of MITF peaks that overlap TFAP2A peaks the MITF
368 binding depends on TFAP2. Such TFAP2-dependent MITF peaks occur both at loci
369 where nucleosome packing depends on TFAP2 (pioneer factor mode) and where it
370 does not (non-pioneer factor mode). At a subset of TFAP2-dependent MITF peaks
371 where TFAP2 acts in pioneer factor mode and characterized by the absence of
372 SOXE binding site TFAP2A binding is, reciprocally, MITF-dependent.

373 **At additional subsets of MITF peaks overlapping TFAP2A peaks, TFAP2**
374 **paralogs inhibit or have no effect on chromatin access for MITF**

375 In Figure 2 we established that at some TFAP2A peaks, TFAP2 paralogs close
376 chromatin, and presumably inhibit binding of transcription factors. Consistent with
377 this prediction, among MITF peaks overlapping TFAP2A peaks, the height of 10%
378 (1,605) was higher in *TFAP2*-KO cells than in WT cells (**Fig. 3A, E; Supplemental**
379 **Fig. S9**). At 58% (924/1,605) of these, the ATAC-seq signal was also significantly
380 higher in *TFAP2*-KO cells versus in WT cells (**violin plot**, **Fig. 3H, H', illustrated in**
381 **Fig. 3H''**). A unique set of transcription factor binding sites, including that for SP1,
382 NFY, JUN and TFE3, were enriched among such elements (**Fig. 3H'''**). Moreover,
383 these elements were modestly associated with TFAP2-inhibited genes**.**

384 Of note, at the majority of MITF peaks that overlap TFAP2A peaks (65%, 10,418/
385 15,752), the height was equivalent in TFAP2-KO and WT cells (**Supplemental Fig.**
386 **S9**). Interestingly TFAP2-independent MITF peaks were not strongly enriched for the
387 TFAP2 binding site (**Supplemental Fig. S11A**), implying that TFAP2 is attracted to
388 many of these sites via other proteins rather than binding directly to the DNA. Such
389 indirect binding may be less avid, as the average height TFAP2-independent MITF
390 peaks was smaller than that of TFAP2-dependent MITF peaks (compare WT MITF
391 signal in (**Supplemental Fig. S9, compare cluster 1 and 4 in WT cells**). As
392 expected, TFAP2-independent MITF peaks were associated neither with TFAP2-
393 activated nor TFAP2-inhibited genes.

394 **TFAP2 and MITF co-regulate genes in the melanocyte gene regulatory network**

395 The delayed pigmentation in zebrafish *tfap2a/tfap2e* double mutants was consistent
396 with two mechanisms which are not exclusive of one another. In the first mechanism,
397 TFAP2 paralogs directly activate *MITF* expression, and thereby indirectly activate
398 expression of pigmentation genes. In the second mechanism, TFAP2 paralogs
399 directly activate expression of pigmentation genes. Supporting the first mechanism,
400 there is a pioneered TFAP2-activated enhancer in intron 2 of the *MITF* gene
401 (**Supplemental Fig. S12**), and *MITF* mRNA levels are about 40% lower in TFAP2-
402 KO cells than in WT cells. However, the first mechanism predicts that loss of TFAP2
403 would most strongly diminish the expression of the most highly MITF-dependent

404 genes. However, many of the genes whose expression was most strongly reduced in
405 *MITF*-KO cells compared to in WT cells were completely TFAP2-independent, or
406 indeed were TFAP2-inhibited (**Supplemental Table 4**). To assess the second
407 mechanism, we identified the set of genes activated directly by MITF, defined as
408 MITF-activated genes associated with an MITF peak, and the set of genes directly
409 activated by TFAP2, defined as TFAP2-activated genes associated with an TFAP2-
410 activated enhancer (i.e., of pioneered or non-pioneered variety). Supporting the
411 second mechanism, genes activated directly both by TFAP2 and by MITF were
412 enriched for GO terms related to pigmentation (**Fig. 4B**), although genes related to
413 pigmentation were among those apparently directly regulated solely by MITF or
414 TFAP2 paralogs (**Fig. 4C**) (Baxter et al., 2019). We took a similar approach to
415 identify genes directly inhibited by TFAP2 and/or by MITF (**Fig. 4D**). Genes directly
416 inhibited by both were strongly enriched for GO terms related to cell adhesion and
417 cell migration (**Fig. 4E**). In summary, reduced expression of pigmentation genes and
418 elevated expression of invasion genes in *TFAP2*-KO cells compared to in WT cells is
419 largely explained by the direct activation and inhibition, respectively, of these
420 categories of genes by TFAP2 paralogs.

421 Considering the strong correlation of TFAP2-inhibited genes with cell migration we
422 performed *in vitro* scratch-recovery-assays and characterized the migrative capacity
423 of our TFAP2-KO cells. Unexpectedly, while WT SK-MEL-28 cells closed the wound
424 after 24 hours, both of our *TFAP2*-KO clones (clone 4.3 and clone 2.12) failed to
425 close the wound within that time (**Supplemental Fig. 13D**). This finding also
426 contrasts with the observation that the expression *tfap2e* correlates negatively with
427 the migratory capacity of zebrafish models of melanoma (Campbell et al., 2021), but
428 it is consistent with the accumulation of melanocytes in the dorsum of zebrafish
429 *tfap2a* knockout embryos (Barrallo-Gimeno et al., 2004; Knight et al., 2004; Knight et
430 al., 2003) and *tfap2a/ tfap2e* double mutant embryos (**Fig. 1, Supplemental Fig.S1**).
431 Furthermore, these results are consistent our previous findings that knocking-down
432 MITF negatively influences cell migration and invasion (Dilshat et al., 2021). The
433 reduced migrative capacity of *TFAP2*-KO cells may be attributed to the strong up-
434 regulation of genes associated with cell adhesion in *TFAP2*-KO cells.

435

436 Finally, we considered how TFAP2 paralogs might regulate the phenotype in
437 melanoma cells. Advanced melanoma is characterized by lower levels of TFAP2A
438 than benign nevi (e.g., Huang et al., 1998), and low transcript levels of *tfap2*
439 paralogs are associated with an invasive phenotype in zebrafish melanoma
440 (Campbell et al., 2021). We examined the association of TFAP2-activated and
441 TFAP2-repressed genes (**Supplemental Fig. 13A-C**) with gene expression profiles
442 from melanoma tumors and melanoma cell lines with distinct phenotypes (Hoek et
443 al., 2008a; Hoek et al., 2006; Jonsson et al., 2010; Rambow et al., 2018; Tirosh et
444 al., 2016; Tsoi et al., 2018; Verfaillie et al., 2015). Enrichment analysis showed (Yu
445 et al., 2012) melanoma profiles previously found to be associated with high levels of
446 MITF activity were enriched for genes directly activated by TFAP2, including the
447 subset associated with TFAP2-dependent MITF peaks (**Fig. 4F**). Moreover,
448 melanoma profiles associated with low levels of MITF activity were enriched for
449 genes directly by TFAP2 (**Fig. 4F**).

450

451 **Discussion**

452

453 In this study, we confirm that Tfap2 paralogs are necessary for timely pigmentation in
454 zebrafish embryos, as well as for normal levels of the expression of pigmentation
455 genes in a melanoma cell line. We also describe how Tfap2 affects expression of
456 such genes, and test the hypothesis that it makes chromatin more accessible to
457 MITF, a transcription factor known to directly regulate the expression of pigmentation
458 genes. The latter involved assessing the consequences of the loss of *MITF* alone,
459 and that of both *TFAP2A* and *TFAP2C*, on global gene expression; on chromatin
460 marks indicative of enhancers, promoters, and repressed chromatin; on nucleosome
461 positioning; and on the binding of TFAP2A to chromatin in *MITF* mutants and that of
462 MITF to chromatin in *TFAP2A/TFAP2C* double mutants. Integration of these
463 datasets yielded a deeper understanding of the mechanisms whereby TFAP2
464 regulates gene expression than could be acquired by more traditional methods.

465

466 Integrating genomic data sets permitted us to identify genomic elements that were
467 bound by TFAP2A in WT cells and that either lost or gained H3K27Ac signal in
468 TFAP2-KO cells; we inferred that these elements were enhancers directly activated

469 or inhibited by TFAP2. Of note, only a minority of TFAP2A peaks coincided with
470 TFAP2-dependent enhancers. As expected by the Tfap2 as pioneer factor model, at
471 a subset of TFAP2A-dependnet enhancers the ATAC-signal was TFAP2-activated.
472 Interestingly, there were elements where the ATAC-seq signal was TFAP2 activated
473 but the H3K27Ac signal independent and such elements were strongly associated
474 with TFAP2-activated genes. It was also interesting that at a subset of TFAP2-
475 inhibited enhancers, loss of TFAP2 led to opening of the chromatin, implying that
476 TFAP2 paralogs recruit distinct transcription factors, and that these in turn recruit
477 either enzymes that open chromatin or enzymes that condense it, in locus-specific
478 fashion. The latter is consistent with findings for FOXA1, which has been shown to
479 recruit proteins that condense chromatin, like GRG3 (Sekiya and Zaret, 2007; Watts
480 et al., 2011).
481
482 A second discovery from our analyses is that TFAP2 can activate enhancers in a
483 non-pioneer factor mode. At a subset of TFAP2A peaks where the H3K27Ac signal
484 was TFAP2-activated, the ATAC-seq signal was TFAP2-independent. Further
485 evidence that such elements are TFAP2-dependent enhancers is that their average
486 H3K4Me3 signal was also TFAP2-dependent. We infer that TFAP2 activates and
487 inhibits these enhancers, but not as a pioneer factor. At such enhancers the
488 continued presence of TFAP2 is necessary for continued acetylation of histone H3
489 lysine 27 (H3K27Ac), which fits with evidence that TFAP2 binds the histone acetyl
490 transferase p300/CBP (Braganca et al., 2003) and inhibits the NURD histone-
491 deacetylase complex (White et al., 2021). TFAP2 may attract other transcription
492 factors without affecting nucleosome positioning; indeed, some TFAP2-dependent
493 MITF peaks were found at Non-pioneered TFAP2- activated enhancers. The fact that
494 the TFAP2 binding site is not strongly enriched at these Non-pioneered TFAP2-
495 activated enhancers may imply that TFAP2 binds these elements indirectly. Finally,
496 we refer to these elements as non-pioneered TFAP2-activated enhancers because
497 in the absence of TFAP2 their activity is lost but chromatin stays open. Our
498 experimental design could not rule out the possibility that TFAP2 stably pioneered
499 these elements such that chromatin remained open (but not active) after TFAP2 was
500 removed. A precedent for this scenario is that at a subset of elements pioneered by
501 PAX7, chromatin remains open after the removal of PAX7 (Mayran et al., 2018).
502 However, the observation that TFAP2 site is less enriched compared to that of

503 pioneered TFAP2-activated enhancers, and that the binding sites of pioneer factors
504 FOS and JUN are enriched (Bejjani et al., 2019), supports the alternative model that
505 such elements are simply pioneered by different transcription factors.
506
507 A third finding from this study is that at a subset of MITF/TFAP2A co-bound peaks,
508 MITF binding was reduced in *TFAP2*-KO cells. A subset of such TFAP2-dependent
509 MITF peaks were present at Pioneered TFAP2-activated enhancers, and at *TFAP2*-
510 independent NDRs (some of which were Non-pioneered TFAP2-activated
511 enhancers, where the mechanism of recruitment of MITF is distinct). Thus, TFAP2
512 modulates MITF activity at certain loci by providing access to chromatin. Of note, at
513 a subset of MITF/TFAP2A peaks, TFAP2 binding was lost in *MITF*-KO cells. There is
514 precedent for reciprocal binding for pioneer factors, in the cases of both FOXA1 and
515 steroid hormone receptors, at subsets of sites where they are co-bound (Swinstead
516 et al., 2016a). Why are all MITF/TFAP2A peaks not mutually dependent? Notably, at
517 many MITF/TFAP2A mutually dependent peaks, the repressive mark H3K27Me3
518 accumulated in MITF-KO cells. This is consistent with evidence a) that the SWI/SNF
519 complex, which MITF probably recruits to such loci, competes for access to
520 chromatin against the Polycomb repressor complex, which deposits H3K27Me3
521 (Wilson et al., 2010), and b) that the binding of pioneer factors is impeded by
522 condensed H3K27me3-positive chromatin (Petruk et al., 2017; Wilson et al., 2010).
523 A possible explanation for this is that at TFAP2-dependent MITF peaks, some
524 measure of BRG1 binding is retained, possibly recruited by another activator like
525 SOX10, in MITF KO cells, but this is not the case for MITF/TFAP2A mutually
526 dependent peaks.
527
528 Finally, our results suggest a mechanism that could account for how TFAP2
529 promotes the pigmentation of embryonic melanophores, the expression of
530 pigmentation genes, and possibly the proliferation of melanoma cells. First, *MITF*
531 expression is lower in *TFAP2*-KO than WT cells. Second, because TFAP2 facilitates
532 binding of MITF to enhancers and promoters of genes that govern pigmentation, the
533 presence of TFAP2 leads to higher expression of those genes. Although the set of
534 MITF-activated but TFAP2-independent genes was not enriched for pigmentation
535 genes, it did include some such genes including *MLANA*, *TYRP1* and *PMEL.*
536 Notably, despite lower MITF mRNA expression in *TFAP2*-KO cells, binding of MITF

537 was unchanged at such genes. This might explain why zebrafish embryonic
538 melanocytes become pigmented more slowly in *tfap2a/tfap2e* double mutants: the
539 number of melanophores in these mutants animals was reduced in embryos
540 depleted for *tfap2a*, singly or in combination with *tfap2e*, and the doubling time of
541 TFAP2-KO cells was longer than that of their WT counterparts. Also, MITF is known
542 to promote proliferation, but whether TFAP2 and MITF cooperate to promote
543 proliferation remains unclear. The expression of genes promoting cell migration and
544 invasion has been observed to be higher in cells with low versus high MITF activity
545 (Rambow et al., 2019). Indeed we show evidence suggesting that TFAP2 paralogs
546 directly suppress such genes, consistent with our previous findings (Campbell et al.,
547 2021). Thus, independent of its other activities as a transcription factor, TFAP2
548 determines which genes can be activated by MITF. In summary, MITF activity in
549 melanoma cells – and thus the phenotypes of these cells – depend in part on the
550 presence of transcription factors that give MITF access to specific regulatory
551 elements.
552
553 **Materials and Methods**
554
555 **Zebrafish lines and maintenance**
556
557 D. rerio were maintained in the University of Iowa Animal Care Facility according to a
558 standard protocol (protocol no. 6011616). All zebrafish experiments were performed
559 in compliance with the ethical regulations of the Institutional Animal Care and Use
560 Committee at the University of Iowa and in compliance with NIH guidelines.
561 Zebrafish embryos were maintained at 28.5℃ and staged by hours or days post-
562 fertilization (hpf or dpf).
563
564
565 **Generation of a zebrafish *tfap2e* loss-of-function allele**
566
567 To generate the tfap2e loss-of-function allele, we designed paired (e.g., left and
568 right) zinc finger nucleases (ZFN) targeting exon 2 of the tfap2e locus resulting in
569 non-homologous end-joining and disruption of the open reading frame for Tfap2e.
570 Briefly, the online tool, ZiFiT (Sander et al., 2010), was used to identify an optimal

571 ZFN target site [utilizing the CoDa approach (Sander et al., 2011). Once identified, a
572 custom DNA fragment encoding the entire left or right zinc finger array (ZFA) along
573 with flanking XbaI and BamHI restriction sites was synthesized (Integrated DNA
574 Technologies, Coralville, IA). Subsequently, the ZFA fragment was subcloned into
575 pMLM290 (Addgene, plasmid 21872), which includes a modified FokI nuclease
576 domain (Miller et al., 2007). Next, the fully assembled ZFN was PCR amplified,
577 directionally cloned into pENTR-D/TOPO (ThermoFisher Scientific), and finally
578 subcloned into pCS2+DEST using Gateway LR Clonase II enzyme mix
579 (ThermoFisher Scientific). Once assembled, the final pCS2+ plasmids were
580 sequence verified, linearized, mRNA synthesized in vitro (mMessage mMachine SP6
581 Kit, Ambion/ThermoFisher Scientific). Synthesized RNA was cleaned using the
582 Qiagen RNeasy Kit (Qiagen) and both left and right ZFN components were co-
583 injected into 1-cell stage zebrafish embryos. Following injections, embryos were
584 initially screened via PCR and restriction enzyme digest to confirm editing at the
585 target site. Upon confirmation, additional embryos from a similar clutch (F0's) were
586 allowed to develop into adulthood, 'mosaics' identified and out-crossed, and a stable
587 F1 generation isolated.
588
589 **Cell lines, reagents, and antibodies**
590
591 The cells referred to as WT throughout the document are the parent SK-MEL-28
592 (HTB-72) line. They and the derivative line, delta6-MITF knockout cells (referred to
593 as MITF-KO cells in this work), were obtained from the laboratory of Dr. Eirikur
594 Steingrimsson. The cells were grown in RPMI 1640 medium (Gibco #5240025)
595 supplemented with 10% FBS (Gibco #10270106) at 5% $CO_2$ and 37°C. Cells were
596 tested for, and determined to be free of, mycoplasma. SK-MEL-28 cells harbor the
597 $BRAF^{V600E}$ and $p53^{L145R}$ mutations (Leroy et al., 2014). The following primary
598 antibodies and their respective dilutions were used in western blotting (WB) and
599 CUT&RUN experiments: anti-Tubulin (Sigma, #T6199), 1:5000 (WB); anti-MITF
600 (Sigma, #HPA003259), 1:2000 (WB), 1:100 (CUT&RUN); anti-TFAP2A (Abcam,
601 ab108311), 1:5000 (WB), 1:200 (CUT&RUN); anti-TFAP2C (Santa-Cruz #SC-12762
602 X ), 1:1000 (WB); anti-H3K27Ac (EMD Millipore, #07-360), 1:100 (CUT&RUN); anti-
603 H3K4Me3 (EMD Millipore, #05-745R), 1:100 (CUT&RUN); H3K27Me3 (EMD
604 Millipore, #07-449), 1:100 (CUT&RUN); Rabbit IgG (EMD Millipore,#12-370), 1:100

605 (CUT&RUN); Mouse IgG (EMD Millipore, #12-371), 1:100 (CUT&RUN). The
606 following secondary antibodies and their respective dilutions were used: Anti-mouse
607 IgG(H+L) DyLight 800 conjugate (Cell Signaling Technologies, #5257), 1:20000; and
608 anti-rabbit IgG(H+L) DyLight 680 conjugate Cell Signaling Technologies, #5366),
609 1:100. Images were captured using an Odyssey CLx Imager (LICOR Biosciences).
610
611
612 **Purification of pA/G-MNase**
613
614 *E.coli* strain BL21-DE3 was transformed with plasmid DNA pAG-MNase-6xHis
615 (Addgene, plasmid #123461). Recombinant pAG-MNase was purified from cells
616 grown in LB medium to OD600 0.6 at 37°C. Cells were induced with 0.5 mM IPTG
617 and cultured for 16 hours at 20°C. Cell pellets were homogenized in lysis buffer (10
618 mM Tris, pH 7.5, 300 mM NaCl, 10 mM imidazole) containing lysozyme and
619 protease inhibitors, then sonicated and the slurry was cleared by centrifugation (35K
620 RPM, Ti70 rotor). The supernatant was subjected to IMAC chromatography (NI-NTA
621 column) and to size-exclusion fractionation (Superdex 75) using a BioLogic DuoFlow
622 QuadTec FPLC system (Bio-Rad). The purified pAG-MNase was concentrated by
623 buffer exchange with ultrafiltration (Amicon Ultra-15, 10K). Finally, the purified pAG-
624 MNase was diluted in dilution buffer (10 mM Tris pH7.5, 120 mM NaCl, 0.01mM
625 EDTA, and 50% glycerol), and stored at -80°C.
626
627 **Generation of *TFAP2A*; *TFAP2C* knockout cell lines (*TFAP2*-KO)**
628
629 *TFAP2*-KO clones were generated using the Alt-R CRISPR-Cas9 technology from
630 Integrated DNA Technologies (IDT). Briefly, crRNAs targeting exon 2 of *TFAP2A* and
631 *TFAP2C* were designed using the Cas9 guide RNA design checker tool (crRNA
632 sequences below). Equimolar concentrations of crRNA and tracrRNA (IDT,
633 #1072532) were annealed to form gRNA complexes. The ribonucleoprotein (RNP)
634 complex was prepared by mixing gRNAs and Cas9 protein (IDT #1081058). SK-
635 MEL-28 cells were transfected with constructs encoding components of RNP
636 complexes using the Lipofectamine CRISPRmax Cas9 transfection reagent
637 (ThermoFisher #CMAX00015) following the manufacturer's protocol. Single-cell
638 colonies were screened by PCR and Sanger sequencing using primers flanking the

639 cut sites (primer sequences below). Mutant clones (clone 2.12 and clone 4.3) were
640 selected and further screened by western blotting, using anti-TFAP2A and anti-
641 TFAP2C antibodies. The control cell lines used in this study were generated
642 following this protocol but without adding gRNA duplexes.
643
644

| **crRNA** | **Sequence (5'-3')** |
|---|---|
| TFAP2A_ex2_gRNA1 | CGTCACGACGGCACCAGCAAGTTTTAGAGCTATGCT |
| TFAP2A_ex2_gRNA2 | CTTACCTCACGCCATCGAGGGTTTTAGAGCTATGCT |
| TFAP2C_ex2_gRNA1 | CGCCACGACGGGAGCAGCAAGTTTTAGAGCTATGCT |
| TFAP2C_ex2_gRNA2 | CCACGACATGCCTCACCAGAGTTTTAGAGCTATGCT |
| **Primers** | **Sequence (5'-3')** |
| TFAP2A_geno_Fw | TCTCTTGTGCCCCCTCCATA |
| TFAP2A_geno_Rv | GCCCACCGACTGTATGTTCCA |
| TFAP2C_geno_Fw | CCGTGACCCCGATTTTGGAT |
| TFAP2C_geno_Rv | CGGCTTCACAGACATAGGCA |

645
646
647 **SDS-PAGE and Western blotting**
648
649 *TFAP2*-KO and WT cells were washed in ice-cold PBS. RIPA buffer containing
650 protease inhibitors (Roche, cOmplete Mini) was added and cells were lysed on ice
651 for 20 minutes. Cell lysates were centrifuged at 14,000 g for 20 minutes and the
652 quantity of protein in the supernatants was quantified using Bradford assays (Bio-
653 Rad #5000002). Laemmli sample buffer (Bio-Rad #1610747, 5% 2-mercaptoethanol)
654 was added to 20 µg protein and samples were boiled at 95°C for 5 minutes before
655 being loaded onto a 10% SDS-polyacrylamide gel (Bio-Rad #4568034). Protein was
656 transferred to polyvinylidene fluoride (PVDF) membranes (Thermo Scientific
657 #88520), which were incubated overnight with primary antibody. Membranes were
658 washed 3 times with TBS-T and incubated with horseradish peroxidase-conjugated
659 anti-rabbit or anti-mouse for 1 hour at room temperature, washed, and imaged using
660 an Amersham Imager 600.
661
662

663
664
665 **ATAC-seq**
666
667 ATAC-seq was performed according to (Buenrostro et al., 2015; Liu et al., 2020) with
668 minor alterations. Briefly, 70,000 *TFAP2*-KO cells (clone 2.12 and clone 4.3, four
669 replicates each) and WT cells (four replicates) were lysed in ice-cold lysis buffer (10
670 mM Tris-HCl, pH 7.4, 10 mM NaCl, 3 mM MgCl2, 0.1% NP-40: Sigma).
671 Transposition was performed directly on nuclei using 25 µl tagmentation reaction mix
672 (Tagment DNA Buffer #15027866, Tagment DNA Enzyme #15027865 from Illumina
673 Tagment DNA kit #20034210). Tagged DNA was subjected to PCR amplification and
674 library indexing, using the NEBNext High-Fidelity 2x PCR Master Mix (New England
675 Biolabs #M0451S) with Nextera DNA CD Indexes (Illumina #20015882), according to
676 the following program: 72℃ for 5 minutes; 98℃ for 30 seconds; 12 cycles of 98℃ for
677 10 seconds, 63℃ for 30 seconds, and 72℃ for 1 minute. The PCR product was
678 purified with 1.8 times the volume of Ampure XP beads (Beckman Coulter #A63881).
679 Library quality was assessed using a BioAnalyzer 2100 High Sensitivity DNA Chip
680 (Agilent Technologies). All DNA libraries that exhibited a nucleosome pattern were
681 pooled and processed for 150bp paired-end sequencing.
682
683
684 **ATAC-seq peak calling and differential analysis**
685
686 ATAC-seq was performed using 150 bp paired-end sequencing reads. Raw ATAC-
687 seq reads were trimmed using Trim Galore Version 0.6.3 (Developed by Felix
688 Krueger at the Babraham Institute) and aligned to human genome assembly hg19
689 (GRCh37) using Bowtie 2 (Langmead and Salzberg, 2012; Langmead et al., 2009)
690 with default parameters. Sorting, removal of PCR duplicates, and identification of
691 fragments shorter than 100 bp as the nucleosome-depleted-regions (NDRs), was
692 performed using BAM filter version 0.5.9. DeepTools version 3.3.0 (Ramírez et al.,
693 2016) was used to check the reproducibility of the biological replicates and generate
694 bigWig coverage files for visualization. Peaks were called using model-based
695 analysis of ChIP-seq 2 (MACS2, version 2.1.1.20160309.6) (Zhang et al., 2008).
696 NDRs for which accessibility differed between *TFAP2*-KO and WT cells were

697 identified using DiffBind version 2.10 (Ross-Innes et al., 2012) with log2 fold-change
698 threshold of >1 and a false discovery rate (FDR) < 0.05. NDRs that are directly
699 regulated by TFAP2 were identified by overlapping differentially accessible NDRs
700 with anti-TFAP2A CUT&RUN peaks; a 1-bp window was used to define overlap.
701 Peaks were assigned to genes using GREAT with a peak-to-gene association rule of
702 the nearest-gene-within-100 kb (McLean et al., 2010). Both the raw ATAC-seq files
703 and processed sequencing data presented in this manuscript have been deposited in
704 the Gene Expression Omnibus (GEO) repository (GSE number pending).
705
706
707 **CUT&RUN**
708
709 CUT&RUN sequencing was performed in *TFAP2*-KO cells (clone 2.12 and clone 4.3,
710 two replicates each) and WT cells (two replicates) as previously described (Meers et
711 al., 2019; Skene and Henikoff, 2017), but with minor modifications. Cells in log-
712 phase culture (approximately 80% confluent) were harvested by cell scraping,
713 centrifuged at 600 g (Eppendorf, centrifuge 5424) and washed twice in calcium-free
714 wash-buffer (20 mM HEPES, pH7.5, 150 mM NaCl, 0.5 mM spermidine, and
715 protease inhibitor cocktail cOmplete Mini, EDTA-free from Roche). Pre-activated
716 concanavalin A-coated magnetic beads (Bangs Laboratories, Inc) were added to cell
717 suspensions ($2x10^5$ cells) and incubated for 15 minutes at 4ºC. Antibody buffer
718 (wash-buffer with 2mM EDTA and 0.05% digitonin) containing anti-TFAP2A, anti-
719 MITF, anti-H3K4Me3, anti-H3K27Me3, anti-H3K27Ac or Rabbit IgG was added and
720 cells were incubated overnight at 4ºC. Cells were washed in dig-wash buffer (wash
721 buffer containing 0.03% digitonin), and pAG-MNase was added at a concentration of
722 500 µg/mL. The pAG-MNase reactions were quenched with 2X Stop Buffer (340mM
723 NaCl, 20mM EDTA, 4mM EGTA, 0.05% digitonin, 100 µg/mL RNAse A (10 mg/mL,
724 Thermo Fisher Scientific #EN0531), 50 µg/mL glycogen (20mg/mL, Thermo Fisher
725 Scientific #R0561) and 2 pg/mL sonicated yeast spike-in control). Released DNA
726 fragments were treated with 1µL/mL phosphatase K (20mg/mL, Thermo Fisher
727 Scientific #25530049) for 1 hour at 50ºC and purified by phenol/chloroform-extraction
728 and ethanol-precipitation. Fragment sizes were analyzed using a 2100 Bioanalyzer
729 (Agilent).
730

731 **CUT&RUN library preparation and data analysis**

732

733 CUT&RUN libraries were prepared using the KAPA Hyper Prep Kit (Roche). Quality
734 control post-library amplification consisted of fragment analysis using the 2100
735 Bioanalyzer (Agilent). Libraries were pooled, brought to equimolar concentrations,
736 and sequenced with 150 bp paired-end reads on an Illumina HiSeq X platform
737 (Novogene, Sacramento, CA). For quality control, paired-end FASTQ files were
738 processed using FastQC (Babraham Bioinformatics). Reads were trimmed using
739 Trim Galore Version 0.6.3 (Developed by Felix Krueger at the Babraham Institute)
740 and then mapped against the hg19 genome assembly using Bowtie2 version 2.1.0
741 (Langmead and Salzberg, 2012; Langmead et al., 2009). The mapping parameters
742 and peak calling of MACS2 peaks (Zhang et al., 2008) were performed as previously
743 described (Meers et al., 2019; Skene and Henikoff, 2017) against their matching
744 control IgG samples. Differential analysis of H3K27Ac and of H3K27Me3 signal in
745 WT and *TFAP2*-KO cells was preformed using MACS2 with a Log2 fold-change
746 threshold of 1, and p-value < $1 \times 10^{-5}$. Differential H3K4Me3, MITF and TFAP2A
747 signal in WT, *TFAP2*-KO and when mentioned *MITF*-KO cells was determined using
748 DiffBind version 2.10.0 (Ross-Innes et al., 2012) with a Log2 fold-change threshold
749 of 1, and FDR < 0.05. DeepTools version 3.3.0 was used to check the reproducibility
750 of the biological replicates, to generate bigwig normalized (RPKM) coverage files for
751 visualization and to plot average CUT&RUN-seq and ATAC-seq profiles (-plotProfile)
752 and generate heatmaps (-plotHeatmap) of normalized reads (Ramírez et al., 2016).
753 MultiBigwigSummary was used to extract read counts (-outRawCounts) (Ramírez et
754 al., 2016) and Prism was used to generate Violin and Box plots. Peaks were
755 assigned to genes using GREAT with a peak-to-gene association rule of the nearest-
756 gene-within-100 kb (McLean et al., 2010)

757

758

759

760 **RNA-seq**

761

762 Four replicate RNA-seq experiments were performed on *TFAP2*-KO cells (clone 2.12
763 and clone 4.3) and WT cells. Total RNA was extracted by direct cell lysis using the
764 RNeasy Plus Mini Kit with QiaShredder (Qiagen #47134). RNA samples with an

765 RNA integrity number (RIN) above nine were used for library generation and 150 bp
766 paired-end sequencing on the Illumina HiSeq2500 platform (Novogene, Sacramento,
767 CA). FASTQ sequence files were processed using FastQC (Babraham
768 Bioinformatics) for quality control, and reads were trimmed using Trim Galore
769 Version 0.6.3 (Developed by Felix Krueger at the Babraham Institute) and
770 subsequently aligned to human genome assembly hg19 (GRCh37) using STAR
771 (Dobin et al., 2013). The output of the --quantMode GeneCounts function of STAR
772 was used for the calculation of differential transcript expression using DESeq2 (Love
773 et al., 2014).The rlog function was used to generate log2-transformed normalized
774 counts. Adjusted p-value < 0.05 was used as the threshold for statistically significant
775 differences. Functional enrichment analyses was performed using PANTHER (Mi et
776 al., 2021). A full list of genes differentially expressed between *TFAP2*-KO and WT
777 cells is provided in Supplemental Table 1-3.
778
779 **Motif analyses**
780
781 Both de novo and known motifs were identified within 200 bp of TFAP2-activated
782 and TFAP2-inhibited enhancer and promoter peak summits using HOMER (-
783 findMotifsGenome).
784
785 **Statistical analysis**
786
787 Fisher's Exact Test was used to assess TFAP2-regulated elements (enhancers and
788 promoters) with TFAP2-regulated gene expression. Data processing and analysis
789 was performed in R and the code can be found at
790 https://GitHub.com/ahelv/Differential_Expression. GraphPad-Prism was used to
791 perform Students t-test as indicated in the figure legends
792
793 **Wound scratch assay**
794
795 A total of 500K cells were seeded per well of 6-well plate (Thermo Scientific, #
796 1483210) to reach confluent monolayer. Cells were incubated in serum free media
797 for 6 hours before wounding with a 200 µL pipette tip. Scratches were manually
798 imaged on an inverted light microscope (Leica #10445930) every 6 hours over a 24-

799 hour time period. The distance of scratch closure between WT and *TFAP2*-KO cells
800 were analyzed with Image J software.
801

Table 1: Hypergeometric analysis: TFAP2 regulated enhancers and gene expression

| Regulatory element (Enhancer) | Effect of TFAP2 on H3K27Ac | Effect of TFAP2 on ATAC | Effect of TFAP2 on RNA-seq | N (# of elements) | OR | LB | UB | p-value All DEG's | p-value \|Log2FC\| >1 |
|---|---|---|---|---|---|---|---|---|---|
| - | Activates | - | Activates | 3,838 | 2.36 | 2.06 | 2.70 | $2.8 \times 10^{-33}$ | $1.12 \times 10^{-14}$ |
| - | Activates | - | Inhibits | 3,838 | 1.03 | 0.85 | 1.24 | $7.0 \times 10^{-01}$ | $5.9 \times 10^{-01}$ |
| - | Inhibits | - | Activates | 1,304 | 1.23 | 0.93 | 1.60 | $1.24 \times 10^{-1}$ | $7.1 \times 10^{-01}$ |
| - | Inhibits | - | Inhibits | 1,304 | 2.30 | 1.87 | 2.82 | $4.95 \times 10^{-14}$ | $4.8 \times 10^{-06}$ |
| Pioneered | Activates | Activates | Activates | 2,002 | 2.60 | 2.23 | 3.06 | $5.44 \times 10^{-29}$ | $6.3 \times 10^{-20}$ |
| Pioneered | Activates | Activates | Inhibits | 2,002 | 1.08 | 0.80 | 1.25 | $9.0 \times 10^{-01}$ | $8.5 \times 10^{-01}$ |
| Non-Pioneered | Activates | Independent | Activates | 1,836 | 1.90 | 1.57 | 2.30 | $2.45 \times 10^{-10}$ | $1.0 \times 10^{-06}$ |
| Non-Pioneered | Activates | Independent | Inhibits | 1,836 | 1.05 | 0.82 | 1.32 | $6.33 \times 10^{-01}$ | $2.8 \times 10^{-01}$ |
| Pioneered | Inhibits | Inhibits | Activates | 864 | 0.68 | 0.33 | 1.251 | $2.9 \times 10^{-01}$ | $1.0 \times 10^{-00}$ |
| Pioneered | Inhibits | Inhibits | Inhibits | 864 | 2.33 | 1.61 | 3.28 | $8.08 \times 10^{-06}$ | $9.44 \times 10^{-05}$ |
| Non-Pioneered | Inhibits | Independent | Activates | 440 | 1.33 | 0.83 | 2.05 | 0.17 | 0.83 |
| Non-Pioneered | Inhibits | Independent | Inhibits | 440 | 1.72 | 1.34 | 2.43 | 0.008 | 0.23 |

OR: odds ratio, LB: lower boundary, UB: upper boundary, ALL DEGs: all differentially expressed genes (FDR < 0.05) in *TFAP2*-KO clones (two independent clones, 4 replicates each) and WT (4 replicates) SK-MEL-28 cells. Log2FC: Log base 2 fold change. N: numbers of TFAP2 regulated enhancer peaks used in the analysis.

802

803

Table 2: Hypergeometric analysis: TFAP2-activated enhancer and promoters, and TFAP2-activated gene expression

| Enhancers and promoters | Effect of TFAP2 on H3K27Ac | Effect of TFAP2 on ATAC | Effect of TFAP2 on RNA-seq | N (# of elements) | OR | LB | UB | p-value Log2FC < -1 |
|---|---|---|---|---|---|---|---|---|
| All peaks | - | - | Activates | 36,948 | 1.66 | 1.40 | 1.98 | $2.4 \times 10^{-08}$ |
| TFAP2A (open chromatin) | - | - | Activates | 26,373 | 1.62 | 1.36 | 1.92 | $1.6 \times 10^{-08}$ |
| TFAP2A peaks | Activates | - | Activates | 4,601 | 3.11 | 2.57 | 3.9 | $6.0 \times 10^{-24}$ |
| TFAP2A peaks | Activates | Independent | Activates | 2,324 | 2.75 | 2.10 | 3.55 | $2.1 \times 10^{-12}$ |
| TFAP2A peaks | - | Activates | Activates | 5,443 | 2.58 | 2.3 | 2.89 | $3.9 \times 10^{-27}$ |
| TFAP2A peaks | Independent | Activates | Activates | 3,241 | 2.97 | 2.73 | 3.70 | $8.8 \times 10^{-19}$ |
| TFAP2A peaks | Activates | Activates | Activates | 2,202 | 4.4 | 3.46 | 5.58 | $4.1 \times 10^{-27}$ |
| TFAP2A peaks | Activates OR | Activates | Activates | 7,842 | 3.80 | 3.1 | 4.60 | $1.44 \times 10^{-35}$ |
| TFAP2A peaks | Independent | Independent | Activates | 19,570 | 1.55 | 1.39 | 1.73 | $6.1 \times 10^{-02}$ |

OR: odds ratio, LB: lower boundary, UB: upper boundary, Log2FC: Log base 2 fold change. Differentially expressed genes in *TFAP2*-KO clones (two independent clones, 4 replicates each) and WT (4 replicates) SK-MEL-28 cells. N: numbers of TFAP2 regulated enhancer and promoter peaks used in the analysis.

804

Table 3: Hypergeometric analysis: TFAP2-inhibited enhancers and promoters, and TFAP2-inhibited gene expression

| Enhancers and promoters | Effect of TFAP2 on H3K27Ac | Effect of TFAP2 on ATAC | Effect of TFAP2 on RNA-seq | N (# of elements) | OR | LB | UB | p-value \|Log2FC\| >1 |
|---|---|---|---|---|---|---|---|---|
| TFAP2A (closed chromatin) | - | - | Inhibits | 12,931 | 1.39 | 1.15 | 1.69 | $8.0 \times 10^{-04}$ |
| TFAP2A (open chromatin) | - | - | Inhibits | 26,373 | 1.06 | 0.90 | 1.25 | $4.8 \times 10^{-01}$ |
| TFAP2A peaks | Inhibits | - | Inhibits | 2,830 | 1.68 | 1.31 | 2.13 | $5.1 \times 10^{-05}$ |
| TFAP2A peaks | - | Inhibits | Inhibits | 4,236 | 1.69 | 1.34 | 2.12 | $1.33 \times 10^{-05}$ |
| TFAP2A peaks | Inhibits | Inhibits | Inhibits | 1,695 | 2.06 | 1.51 | 2.76 | $8.47 \times 10^{-06}$ |
| TFAP2A peaks | Inhibits OR | Inhibits | Inhibits | 5,371 | 1.68 | 1.38 | 2.03 | $3.61 \times 10^{-07}$ |
| TFAP2A peaks | Independent | Independent | Inhibited | 21,848 | 0.98 | 0.82 | 1.15 | $7.0 \times 10^{-01}$ |

OR: odds ratio, LB: lower boundary, UB: upper boundary, Log2FC: Log base 2 fold change. Differentially expressed genes in *TFAP2*-KO clones (two independent clones, 4 replicates each) and WT (4 replicates) SK-MEL-28 cells. N: numbers of TFAP2 regulated enhancer and promoter peaks used in the analysis.

805

Table 4: Hypergeometric analysis: TFAP2-dependent MITF peaks and gene expression

| TFAP2's effect on: MITF | Effect of TFAP2 on ATAC | Effect of TFAP2 on RNA-seq | N (# of elements) | OR | LB | UB | p-value All DEG's | p-value \|Log2FC\| >1 |
|---|---|---|---|---|---|---|---|---|
| TFAP2-dependent | - | Activates | 5,443 | 2.96 | 2.56 | 3.43 | $3.47 \times 10^{-41}$ | $8.4 \times 10^{-26}$ |
| TFAP2-dependent | - | Inhibits | 5,443 | 1.00 | 0.81 | 1.23 | $9.5 \times 10^{-01}$ | $7.2 \times 10^{-01}$ |
| TFAP2-dependent | Activates | Activates | 3,083 | 3.43 | 2.95 | 3.98 | $3.19 \times 10^{-49}$ | $1.16 \times 10^{-26}$ |
| TFAP2-dependent | Activates | Inhibits | 3,083 | 1.15 | 0.92 | 1.42 | $1.7 \times 10^{-01}$ | $4.0 \times 10^{-01}$ |
| TFAP2-dependent | Independent | Activates | 2,358 | 2.38 | 1.81 | 2.55 | $1.6 \times 10^{-16}$ | $1.07 \times 10^{-13}$ |
| TFAP2-dependent | Independent | Inhibits | 2,358 | 1.13 | 0.91 | 1.40 | $2.3 \times 10^{-01}$ | $4.0 \times 10^{-01}$ |
| Mutually dependent | Activates | Activates | 717 | 2.967 | 1.768 | 4.756 | $3.47 \times 10^{-05}$ | $9.28 \times 10^{-05}$ |
| Mutually dependent | Activates | Inhibits | 717 | 0.789 | 0.284 | 1.772 | $7.07 \times 10^{-01}$ | 1.00 |
| TFAP2-inhibited | Inhibits | Activates | 924 | 0.73 | 0.48 | 1.06 | $1.11 \times 10^{-01}$ | 1.00 |
| TFAP2-inhibited | Inhibits | Inhibits | 924 | 2.75 | 2.21 | 3.39 | $1.1 \times 10^{-17}$ | $3.5 \times 10^{-04}$ |
| TFAP2-inhibited | Independent | Activates | 681 | 1.18 | 0.80 | 1.68 | 1.00 | 1.00 |
| TFAP2-inhibited | Independent | Inhibits | 681 | 2.27 | 1.72 | 2.94 | $2.9 \times 10^{-08}$ | $1.2 \times 10^{-02}$ |

OR: odds ratio, LB: lower boundary, UB: upper boundary, ALL DEGs: all differentially expressed genes in *TFAP2*-KO clones (two independent clones, 4 replicates each) and WT (4 replicates) SK-MEL-28 cells. Log2C: Log base 2 fold change. N: numbers of TFAP2–dependent MITF peaks used in the analysis.

806

807

Fig 1

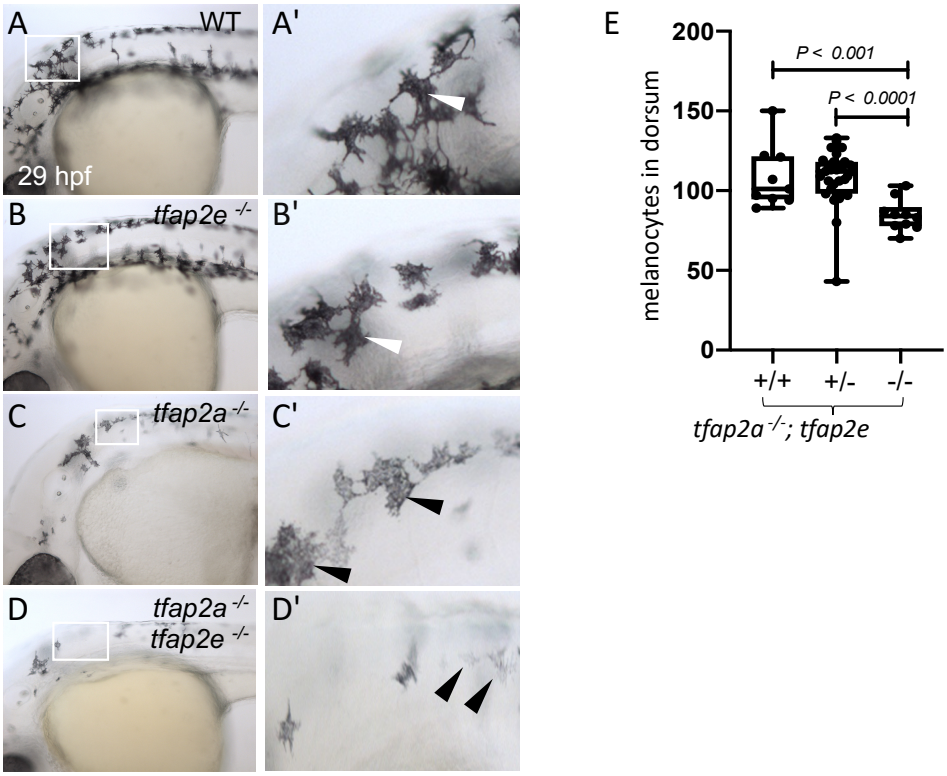
A
WT
29 hpf
A'
B
tfap2e -/-
B'
C
tfap2a -/-
C'
D
tfap2a -/-
tfap2e -/-
D'
E
melanocytes in dorsum
200
150
100
50
0
P < 0.001
P < 0.0001
+/+
+/-
-/-
tfap2a -/-; tfap2e

808

809

Fig. 2

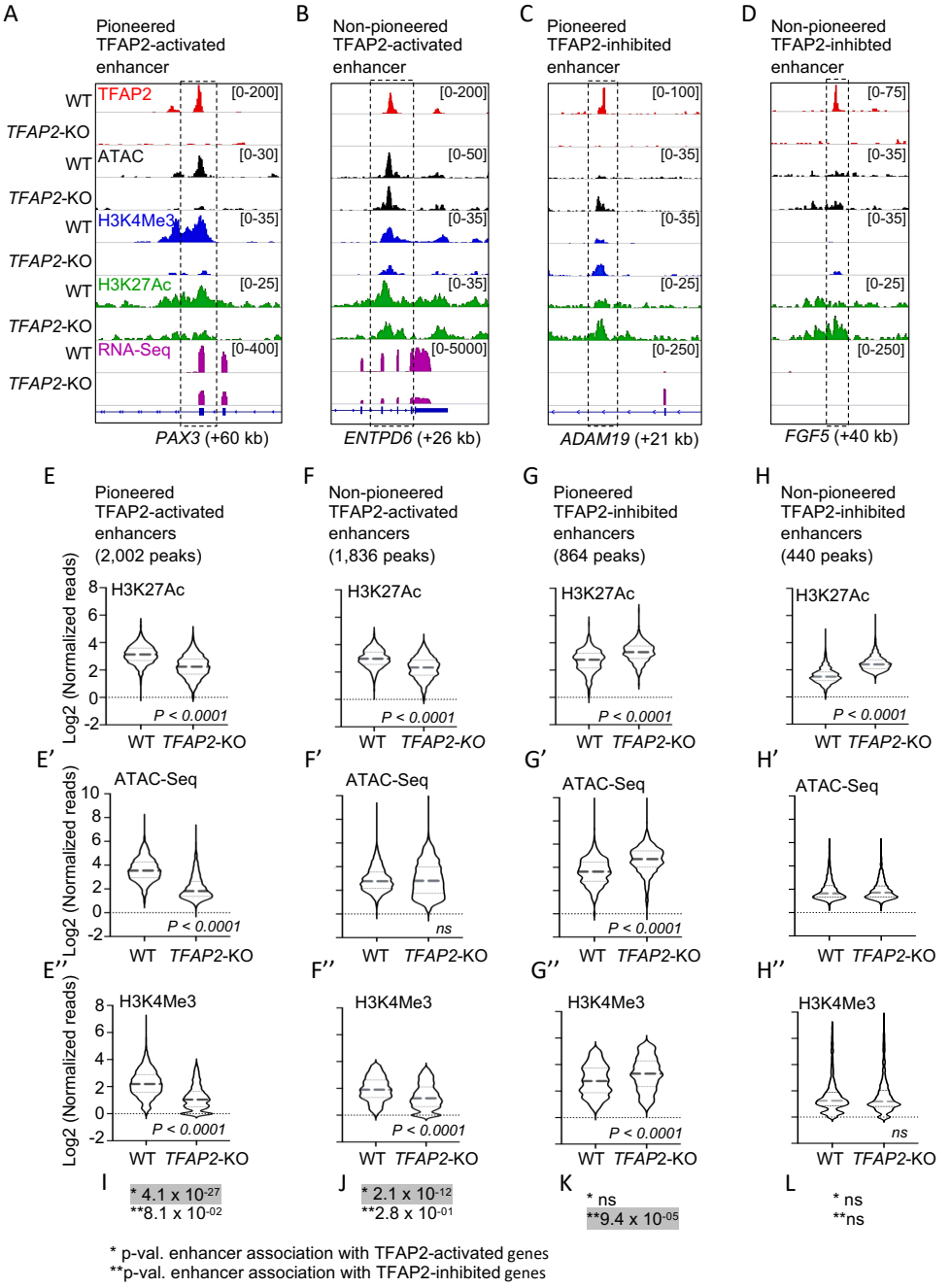


M

Pioneered TFAP2-activated enhancers

| Motif | TF | Rank | P-value |
|---|---|---|---|
| | TFAP2 | 1,2 | 1 x $10^{-600}$ |
| | EBF | 3 | 1 x $10^{-51}$ |
| | SOXE | 4,6 | 1 x $10^{-36}$ |
| | RUNX | 7 | 1 x $10^{-31}$ |
| | MITF | 28 | 1 x $10^{-12}$ |

N

Non-pioneered TFAP2-activated enhancers

| Motif | TF | Rank | P-value |
|---|---|---|---|
| | TFAP2 | 1 | 1 x $10^{-280}$ |
| | FRA1 | 2 | 1 x $10^{-46}$ |
| | RUNX | 4 | 1 x $10^{-27}$ |
| | TEAD | 6 | 1 x $10^{-24}$ |
| | ZFX | 7 | 1 x $10^{-22}$ |

O

Pioneered TFAP2-inhibited enhancers

| Motif | TF | Rank | P-value |
|---|---|---|---|
| | TFAP2 | 1,2 | 1 x $10^{-63}$ |
| | RUNX | 3 | 1 x $10^{-37}$ |
| | CST6 | 4 | 1 x $10^{-21}$ |
| | ETS1 | 6 | 1 x $10^{-14}$ |
| | CTCF | 12 | 1 x $10^{-12}$ |

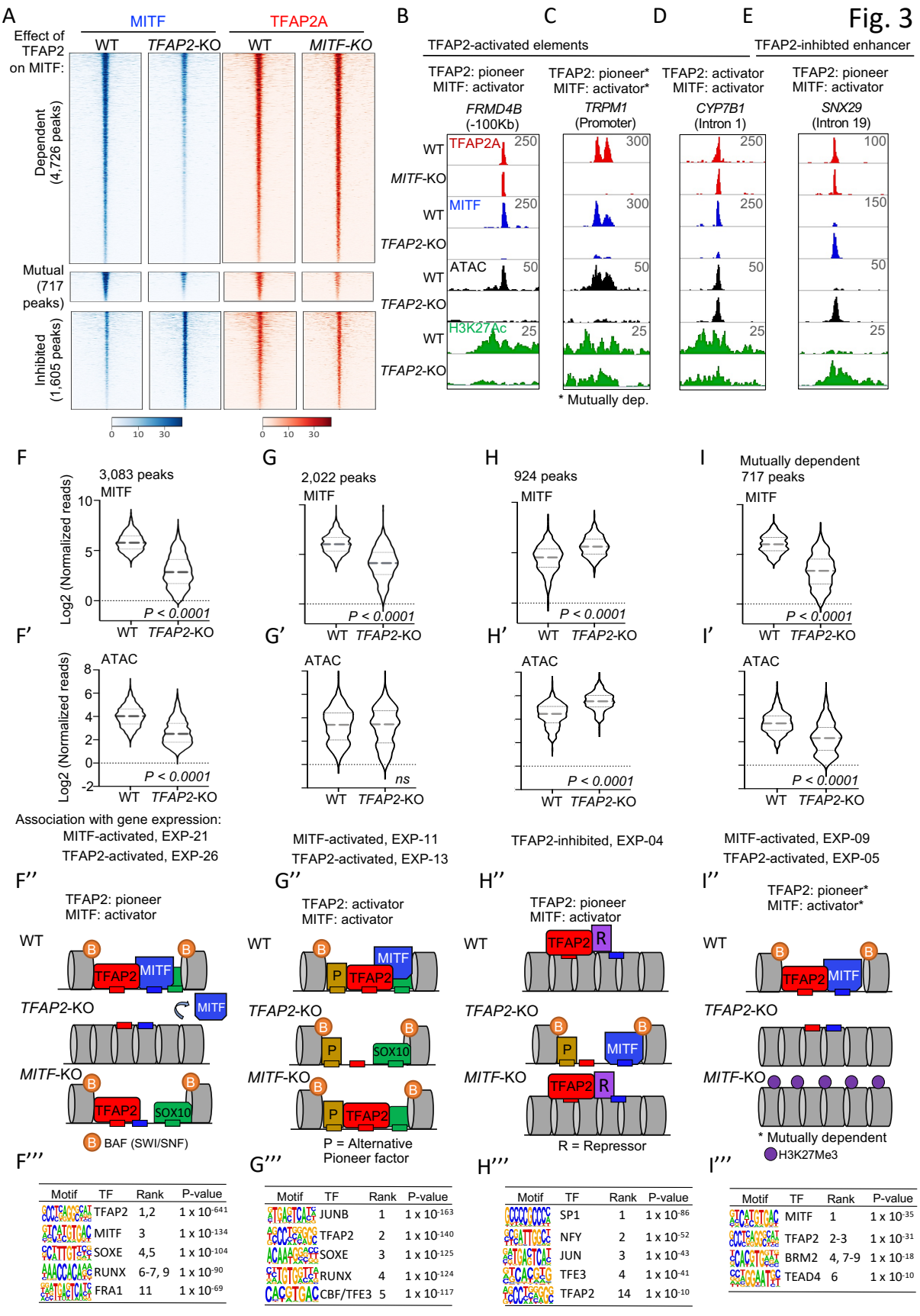
Fig. 3
A
MITF
TFAP2A
Effect of TFAP2 on MITF:
WT
TFAP2-KO
WT
MITF-KO
Dependent (4,726 peaks)
Mutual (717 peaks)
Inhibited (1,605 peaks)
B
C
D
E
TFAP2-activated elements
TFAP2-inhibted enhancer
TFAP2: pioneer
MITF: activator
TFAP2: pioneer*
MITF: activator*
TFAP2: activator
MITF: activator
TFAP2: pioneer
MITF: activator
FRMD4B (-100Kb)
TRPM1 (Promoter)
CYP7B1 (Intron 1)
SNX29 (Intron 19)
TFAP2A
MITF
ATAC
H3K27Ac
* Mutually dep.
F
3,083 peaks
MITF
Log2 (Normalized reads)
P < 0.0001
G
2,022 peaks
H
924 peaks
I
Mutually dependent 717 peaks
F'
G'
H'
I'
ATAC
ns
Association with gene expression:
MITF-activated, EXP-21
TFAP2-activated, EXP-26
MITF-activated, EXP-11
TFAP2-activated, EXP-13
TFAP2-inhibited, EXP-04
MITF-activated, EXP-09
TFAP2-activated, EXP-05
F''
G''
H''
I''
TFAP2: pioneer
MITF: activator
TFAP2: activator
MITF: activator
TFAP2: pioneer
MITF: activator
TFAP2: pioneer*
MITF: activator*
TFAP2-KO
MITF-KO
BAF (SWI/SNF)
P = Alternative Pioneer factor
R = Repressor
* Mutually dependent
H3K27Me3
F'''
G'''
H'''
I'''
Motif TF Rank P-value
TFAP2 1,2 1 x 10-641
MITF 3 1 x 10-134
SOXE 4,5 1 x 10-104
RUNX 6-7, 9 1 x 10-90
FRA1 11 1 x 10-69
Motif TF Rank P-value
JUNB 1 1 x 10-163
TFAP2 2 1 x 10-140
SOXE 3 1 x 10-125
RUNX 4 1 x 10-124
CBF/TFE3 5 1 x 10-117
Motif TF Rank P-value
SP1 1 1 x 10-86
NFY 2 1 x 10-52
JUN 3 1 x 10-43
TFE3 4 1 x 10-41
TFAP2 14 1 x 10-10
Motif TF Rank P-value
MITF 1 1 x 10-35
TFAP2 2-3 1 x 10-31
BRM2 4, 7-9 1 x 10-18
TEAD4 6 1 x 10-10

812

Fig. 4

A

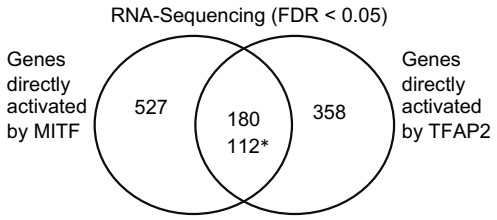


*Associated with a TFAP2-dependent MITF peak

D

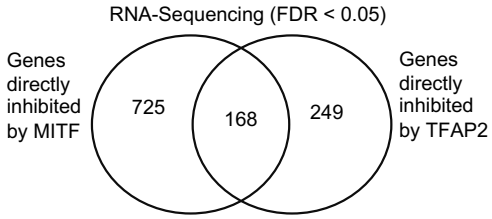


B

MITF and TFAP2-activated genes (Top 5 hits)

| GO biological process | Enrichment | No. of genes | FDR |
|---|---|---|---|
| Pigmentation | 16.75 | 11 | $2.79 \times 10^{-06}$ |
| Pigment differentiation | 28.02 | 6 | $9.79 \times 10^{-04}$ |
| Cell differentiation | 44 | 77 | $8.7 \times 10^{-03}$ |
| Cellular pigmentation | 13.49 | 5 | $4.68 \times 10^{-02}$ |
| Receptor signaling | 3.51 | 15 | $3.78 \times 10^{-02}$ |

E

MITF and TFAP2-inhibited genes (Top 5 hits)

| GO biological process | Enrichment | No. of genes | FDR |
|---|---|---|---|
| Vasculature development | 6.8 | 32 | $1.8 \times 10^{-12}$ |
| Tube development | 5.13 | 36 | $1.4 \times 10^{-10}$ |
| Cell motility | 4.81 | 34 | $2.2 \times 10^{-08}$ |
| Cell migration | 3.51 | 31 | $3.7 \times 10^{-07}$ |
| Cell adhesion | 3.5 | 20 | $7.0 \times 10^{-06}$ |

C

Pigmentation related genes directly activated by:

| **MITF** | **MITF and TFAP2** | **TFAP2** |
|---|---|---|
| *DKC1* | *RAB1A* | *IGFBP7* |
| *MLANA* | *RAB32* | *KCTD15* |
| *EIF3B* | *HPS3* | *ABCA12* |
| *KBTBD8* | *CLCN7* | *CHD7* |
| *RAB27A* | *CTNNB1* | *EDNRB* |
| *STX3* | *CTSD* | *EN1* |
| *AFG3L2* | *DCT* | *HIPK2* |
| *BNC2* | *ETS1* | *HTRA1* |
| *CCT2* | *GPR143* | *MCM4* |
| *DTNBP1* | *MAFB* | *MYO5A* |
| *IRF4* | *MFSD12* | *PARN* |
| *MLPH* | *MITF* | *PAX3* |
| *MYO10* | *MREG* | *RAD21* |
| *OSTM1* | *NR4A3* | *SDC2* |
| *PARD3* | *OCA2* | *SLC2A11* |
| *PMEL* | *PEPD* | *SOX9* |
| *PPARGC1A* | *RAB38* | *SYTL2* |
| *PSEN2* | *SH3BP4* | *TFAP2C* |
| *RPS14* | *SH3PXD2A* | *ALCAM* |
| *RPS7* | *SNAI2* | *BLM* |
| *SCUBE2* | *TRPM1* | *DISC1* |
| *SLC45A2* | *VDR* | *ERBB3* |
| *STXBP1* | | *FANCC* |
| *SZT2* | | *LYST* |
| *TYRP1* | | *MIB1* |
| *USF2* | | *NBN* |
| *VPS18* | | *PMCH* |
| | | *PRKDC* |
| | | *SOX5* |

F

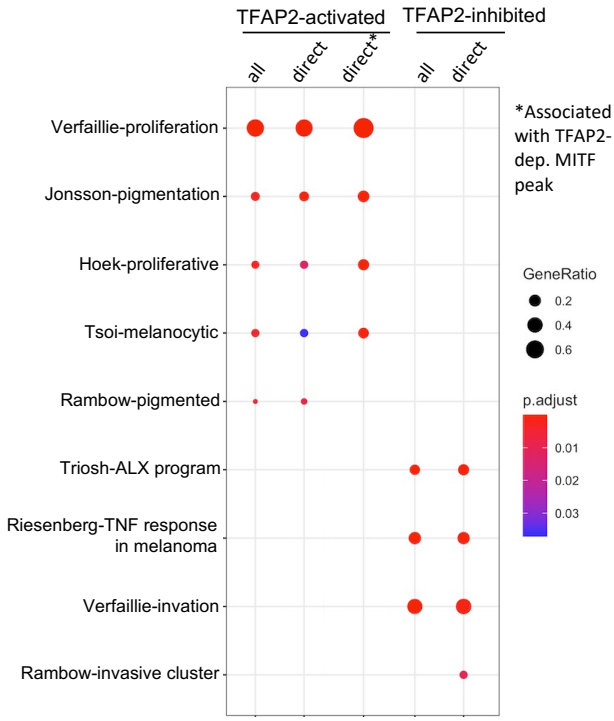


813

814 **Figure legends**

815

816 **Figure 1: Stable KO of *tfap2e* has no effect on pigmentation in WT embryos but**
817 **alters melanocyte development and delays melanin synthesis in *tfap2a***
818 **mutants. (A-D)** Lateral views of head and trunk of live embryos at 29 hpf, anterior to
819 the left and dorsal to the top. **(A-A')** A WT (sibling) embryo with normal melanocytes
820 (white arrowhead). **(B-B')** A *tfap2e*$^{ui157ui/157}$ embryo, with melanocytes that are normal
821 in terms of number, differentiation and pigmentation (white arrowhead). **(C-C')** A
822 *tfap2a*$^{low/low}$ homozygous mutant embryo, with fewer melanocytes than its
823 *tfap2e*$^{157/157}$ and WT sibling embryos. **(D-D')** A *tfap2a*$^{low/low}$*; tfap2e*$^{157/157}$ double-
824 mutant embryo, with fewer melanin-producing melanophores than its *tfap2a*$^{low/low}$
825 sibling. **(E)** Box plot illustrating the number of pigmented melanocytes in the dorsum
826 of WT (+/+), *tfap2a* mutant, *tfap2e* mutant, and double *tfap2a; tfpa2e* mutant
827 embryos at 36 hpf. Center line, mean; box limits, upper and lower quartiles;
828 whiskers, minimum and maximum values; black dots, number of melanocytes per
829 individual embryo (WT; n=9, *tfap2a*$^{low/low}$*;tfap2e*$^{+/157}$, n=32; *tfap2a*$^{low/low}$*;tfap2e*$^{157/157}$,
830 n=10). P-value according to the Student's t-test.

831

832 **Figure 2: TFAP2 paralogs facilitate gene expression by opening and**
833 **condensing chromatin. (A-D)** Screenshot of IGV genome browser
834 (GRCH37/hg19), visualizing anti-TFAP2A CUT&RUN-seq (red), ATAC-seq (black),
835 anti-H3K4Me3 CUT&RUN-seq (blue), anti-H3K27Ac CUT&RUN-seq (green) and
836 RNA-seq (magenta) datasets at **(A)** a pioneered TFAP2-activated enhancer at the
837 *PAX3* (+60 kb) locus **(B)** a non-pioneered TFAP2A-activated enhancer at the
838 *ENTPD6* (+26kb) locus **(C)** a pioneered TFAP2-inhibited enhancer at the *ADAM19*
839 (+21 kb) locus and **(D)** a non-pioneered TFAP2A-inhibited enhancer at the *FGF5*
840 (+40kb) locus. Genotypes as labeled; y-axes are grouped scaled per dataset. **(E-E'')**
841 Violin plots representing **(E)** anti-H3K27Ac (two independent replicates) **(E')** ATAC-
842 seq (four independent replicates) and **(E'')** anti-H3K4Me3 (two independent
843 replicates) normalized reads at pioneered TFAP2-activated enhancers. **(F-F'')** Violin
844 plots representing **(F)** anti-H3K27Ac **(F')** ATAC-seq and **(E'')** anti-H3K4Me3
845 normalized reads at non-pioneered TFAP2-activated enhancers. **(G-G'')** Violin plots
846 representing **(G)** anti-H3K27Ac **(G')** ATAC-seq and **(G'')** anti-H3K4Me3 normalized
847 reads at pioneered TFAP2-inhibited enhancers. **(H-H'')** Violin plots representing **(H)**

848 anti-H3K27Ac **(H')** ATAC-seq and **(H'')** anti-H3K4Me3 normalized reads at non-
849 pioneered TFAP2-inhibited enhancers. P-values shown were determined by
850 Students t-test. **(I-L)** Hypergeometric analysis of TFAP2 regulated enhancers at
851 TFAP2-activated (*) and TFAP2-inhibited (**) genes in *TFAP2*-KO cells (FDR < 0.05,
852 |log2FC| > 1). **(M-O)** Enrichment of transcription factor motifs at (M) pioneered
853 TFAP2-activated enhancers, at (N) non-pioneered TFAP2-activated enhancers and
854 at (O) pioneered TFAP2-inhibited enhancers as determined using HOMER motif
855 analysis. P values were calculated using ZOOPS scoring (zero or one occurrence
856 per sequence) coupled with hypergeometric enrichment analysis. TF; transcription
857 factor.
858
859 **Figure 3: TFAP2 paralogs facilitate chromatin access by MITF. (A)** Density
860 heatmaps of anti-MITF CUT&RUN-seq in SK-MEL-28 and *TFAP2*-KO cells, and anti-
861 TFAP2 CUT&RUN-seq in SK-MEL-28 and *MITF*-KO cells at TFAP2-dependent MITF
862 peaks (top), mutually dependent peaks (center) and TFAP2-inhibited MITF peaks
863 (bottom). Number of peaks in each group as labelled. Regions shown are +/- 3 kb
864 from peak center, normalized reads (RPKM). **(B-E)** Screenshot of IGV genome
865 browser (GRCH37/hg19), showing anti-TFAP2A (red) CUT&RUN-seq in SK-MEL-28
866 and *MITF*-KO cells, and anti-MITF (blue) CUT&RUN-seq, ATAC-seq (black) and
867 anti-H3K27Ac (green) CUT&RUN-seq profiles in SK-MEL-28 and *TFAP2*-KO cells.
868 Examples of MITF binding at **(B-D)** TFAP2-activated and **(E)** TFAP2-inhibted
869 regulatory elements. Genotypes as labeled; y-axes are grouped scaled per dataset.
870 **(F-F')** Violin plot representing **(F)** anti-MITF CUT&RUN-seq (two independent
871 replicates) and **(F')** ATAC-seq (four independent replicates) at 3,083 pioneered
872 TFAP2-activated MITF peaks. **(G-G')** Violin plot representing **(G)** anti-MITF
873 CUT&RUN-seq and **(G')** ATAC-seq at 2,022 non-pioneered TFAP2-activated MITF
874 peaks. **(H-H')** Violin plot representing **(H)** anti-MITF CUT&RUN-seq and **(H')** ATAC-
875 seq at 924 pioneered TFAP2-inhibited MITF peaks and **(I-I')** Violin plot representing
876 **(I)** anti-MITF CUT&RUN-seq and **(I')** ATAC-seq at 717 mutually dependent peaks. P-
877 value according to Students t-test, ns; not statistically significant, normalized reads
878 RPKM. Association with gene expression; hypergeometric analysis of TFAP2-
879 depednent and TFAP2-inhibited MITF peaks are shown at TFAP2-activated and
880 MITF-activated genes (FDR < 0.05, log2FC > |1|). **(F''- I'')** Schematic representation
881 of TFAP2-dependent and TFAP2-inhibited MITF peaks as labelled; B; BAF complex

882 (SWI/SNF), P; alternative pioneer factor. R; repressor protein. Transcription factor
883 binding sites indicated by small rectangles, TFAP2 (red), MITF (blue) and alternative
884 pioneer factor (yellow), example activator SOX10 (green) . **(F''' – I''')** Enrichment of
885 transcription factor motifs using HOMER at (F''') pioneered TFAP2-dependent MITF
886 peaks, (G''') non-pioneered TFAP2-dependent MITF peaks, (H''') TFAP2-inhibited
887 MITF peaks and **(I''')** mutually dependent peaks. P values were calculated using
888 ZOOPS scoring (zero or one occurrence per sequence) coupled with hypergeometric
889 enrichment analysis. TF; transcription factor.
890
891 **Figure 4: TFAP2 and MITF co-regulate pigmentation and cell differentiation**
892 **genes in SK-MEL-28 cell lines. (A)** Venn diagram representing directly MITF
893 activated genes (MITF peaks within 100Kb of a TSS), based on RNA-seq, in *MITF*-
894 KO verses WT cells (FDR < 0.05) and genes directly activated by TFAP2 (TFAP2-
895 activated enhancers within 100Kb of a TSS), based on RNA-seq, with TFAP2-
896 activated enhancers, in *TFAP2*-KO verses WT cells (FDR < 0.05). The number of
897 overlapping genes with TFAP2-dependent MITF peaks are also shown (*). **(B)** Gene
898 ontology (GO) biological process analysis (Top 5 hits) that are enriched among
899 MITF- and TFAP2-activated genes. **(C)** A curated list of pigment-associated genes
900 (Baxter et al., 2009) was intersected with directly MITF-activated, directly
901 MITF/TFAP2-activated, and TFAP2-acitvated genes and represented by gene list.
902 **(D)** Venn diagram representing directly MITF inhibited genes, based on RNA-seq, in
903 *MITF*-KO verses WT cells (FDR < 0.05) and genes directly inhibited by TFAP2,
904 based on RNA-seq, with TFAP2-inhibited enhancers, in *TFAP2*-KO verses WT cells
905 (FDR < 0.05). **(E)** Gene ontology (GO) biological process analysis (Top 5 hits) that
906 are enriched among MITF- and TFAP2-inhibited genes. GO analysis was performed
907 using PANTHER. **(F)** Dot plot of enrichment analysis showing the enrichment of
908 gene signatures from the literature in directly TFAP2-activated and TFAP2-inhibted
909 genes, based on RNA-seq, in *TFAP2*-KO and SK-MEL-28 cells. P value is red
910 lowest to blue highest; gene ratio is the ratio between genes and all genes in the GO
911 category. Analysis of directly TFAP2-activated genes associated with TFAP2-
912 dependent MITF peaks are shown (*).
913
914 **Figure S1: *tfap2e* mutant zebrafish do not display a melanocyte phenotype**
915 **whereas *tfap2a/e* double mutant zebrafish display a significant reduction in**

916 **melanocyte number**. **(A)** A 157 base pair mutation at the end of tfap2e exon 2
917 disrupts splicing and results in a premature stop codon. **(B)** PCR using primers in
918 tfap2e exon 2 and intron 2 (e2-i2) amplifies a band of the expected 450 base pair
919 size in tfap2e mutants but not wildtype (WT), whereas primers in exon 2 and exon 3
920 (e2-e3) amplify only in wildtype. NTC: not template control. **(C)** qRT-PCR analysis of
921 tfap2e expression shows that the transcript is strongly decreased in *tfap2e*-/-
922 mutants, consistent with nonsense-mediated decay (Student's t-test, **** $p<0.0001$).
923 **(D-E)** tfap2e mutant zebrafish at 36 hpf, *tfap2e*+/- **(D)** and *tfap2e*-/- **(E)** are
924 phenotypically indistinguishable. **(F)** Histogram illustrating the number of pigmented
925 melanocytes in the dorsum of *tfap2e*+/- and *tfap2e*-/- mutant zebrafish embryos,
926 **(G-H)** Zebrafish embryos from a *tfap2a*+/-;*tfap2e*+/- incross at 48 hpf. **(G)** A wildtype
927 embryo shows normal melanocyte patterning. **(H)** A tfap2a-/- mutant embryo has
928 fewer and paler embryonic melanocytes than wildtype**. (I)** tfap2a-/-;tfap2e+/- and (J)
929 tfap2a-/- ;tfap2e-/- appear phenotypically indistinguishable from tfap2a-/- at 48 hpf.
930
931 **Figure S2: TFAP2 binds to open and closed chromatin. (A)** Screenshot of IGV
932 genome browser (GRCH37/hg19), visualizing anti-TFAP2A and IgG CUT&RUN-seq
933 profiles. Peaks were called using MACS2 software (two independent replicates) and
934 are illustrated by blue bars under the anti-TFAP2A track. **(B)** Density heatmap
935 centred on the 36,867 TFAP2A peaks identified by anti-TFAP2A CUT&RUN in WT
936 SK-MEL-28 cells. Regions shown are +/- 3 kb from peak center, Peaks were
937 grouped by distance to an annotated transcriptional start site. Promoter peaks +/-
938 3kb from a TSS and enhancers >3 kb from an TSS. Anti-TFAP2A, anti-H3K4Me3
939 and anti-H3K27Ac CUT&RUN-seq, and ATAC-Seq profiles are shown. Normalized
940 reads (RPKM). **(C)** Histogram representing H3K27Ac signal, binned from low-high
941 read-depth on the x-axis and percentage of TFAP2A promoter peaks (black) and
942 TFAP2A enhancer peaks (red) on the y-axis. **(D)** Violin plots illustrating TFAP2A and
943 IgG normalized reads (RPKM) at nucleosome depleted regions (ATAC-peaks) and at
944 nucleosome occupied DNA (no ATAC-peak) **(E)** Density heatmap representing
945 TFAP2A CUT&RUN and ATAC-seq profiles at TFAP2A peaks that overlap
946 nucleosome depleted regions (ATAC-peaks) and at nucleosome bound DNA (no
947 ATAC-peak), the number of TFAP2A peaks in each group are as labeled.
948

949 **Figure S3: Example loci of TFAP2A peaks at open and closed chromatin. (A-B)**
950 IGV screenshots of TFAP2A peaks that **(A)** closed chromatin and **(B)** open
951 chromatin, based on ATAC-seq, in SK-MEL-28 cells. Genes names and distance to
952 a transcriptional start site as labeled. **(C)** HOMER motif analysis at TFAP2A peaks at
953 closed chromatin and **(D)** at open chromatin. TF, transcription factors; the top
954 ranking transcription factor motif is shown, with P-values calculated with HOMER-
955 based hypergeometric enrichment analysis.
956
957 **Figure S4: Generation of TFAP2A; TFAP2C double mutant SK-MEL-28 cell**
958 **lines. (A)** RNA-seq showing transcript counts of TFAP2 paralogs in SK-MEL-28
959 cells. Transcript counts for WT cells (n=4) and two *TFAP2A;TFAP2C* double
960 knockout clones (4 replicates each) are shown. The expression of WT and mutant
961 alleles of *TFAP2A* is comparable between cell lines whereas mutant alleles of
962 *TFAP2C* are strongly reduced. **(B)** Two guide RNAs (crRNAs) each were designed
963 to target exon 2 of *TFAP2A* and *TFAP2C* (yellow boxes). **(C)** A 401 base pair
964 inversion and a 452 base pair deletion at exon 2 of *TFAP2A* and *TFAP2C*,
965 respectively, was identified in clone 4.3. *TFAP2A* and *TFAP2C* mutant alleles
966 resulted in a frame-shift and premature stop codon in alleles of both genes. **(D)** A
967 405 base pair deletion at exon 2 of *TFAP2A* resulted in a frame-shift and premature
968 stop codon in clone 2.12. A 455 base pair deletion, and a 70 base pair insertion, 1
969 base pair deletion (Indel) was identified in exon 2 of *TFAP2C*. Such mutations
970 resulted in a frame-shift and premature stop codon. Additional permutations were not
971 identified at exon 2 of *TFAP2A* or *TFAP2C* in clone 4.3 or clone 2.12 cells. Inv;
972 inversion, Del; deletion. **(E)** Western blot analysis confirming loss of TFAP2A and
973 TFAP2C immunoactivity in clone 4.3 and clone 2.12 cell lines.
974
975 **Figure S5: TFAP2 paralogs activate and inhibit gene expression directly.**
976 **(A)** Volcano plot illustrating differential gene expression as determined by RNA
977 sequencing of *TFAP2*-KO cells (two independent clones (2.12 and 4.3); four
978 replicates each) versus WT cells (SK-MEL-28; four replicates). Log2 fold change
979 (FC) of mean transcript levels on the x-axis and log2 p-value on the y-axis. Red dots
980 represent direct target genes of TFAP2A that are differentially expressed (FDR <
981 0.05, log2FC > |1|), as determined by anti-TFAP2 CUT&RUN in SK-MEL-28 cells.
982 Gray dots represent genes that are differentially expressed but not bound by TFAP2.

983 The number and percentage of genes that are regulated by TFAP2 are specified.
984 Directly TFAP2A-dependent genes were identified based on the gene-association
985 rule (single nearest gene within 100 kb of a transcription start site).
986
987 **Figure S6: TFAP2 paralogs directly activate and inhibit promoters as pioneer**
988 **factors. (A-D)** Screenshot of IGV genome browser (GRCH37/hg19), visualizing anti-
989 TFAP2A CUT&RUN-seq (red), ATAC-seq (black), anti-H3K4Me3 CUT&RUN-seq
990 (turquoise), anti-H3K27Ac CUT&RUN-seq (green) and RNA-seq (magenta) datasets
991 at **(A-B)** TFAP2-activated promoters and **(C-D)** TFAP2-inhibited promoters.
992 Genotypes as labeled; y-axes are grouped scaled per dataset. **(E-E'')** Violin plots
993 representing **(E)** anti-H3K27Ac (two independent replicates) **(E')** ATAC-seq (four
994 independent replicates) and **(E'')** anti-H3K4Me3 (two independent replicates)
995 normalized reads at pioneered TFAP2-activated promoters. **(F-F'')** Violin plots
996 representing **(F)** anti-H3K27Ac **(F')** ATAC-seq and **(E'')** anti-H3K4Me3 normalized
997 reads at non-pioneered TFAP2-activated promoters. **(G-G'')** Violin plots representing
998 **(G)** anti-H3K27Ac **(G')** ATAC-seq and **(G'')** anti-H3K4Me3 normalized reads at
999 pioneered TFAP2-inhibited promoters. **(H-H'')** Violin plots representing **(H)** anti-
1000 H3K27Ac **(H')** ATAC-seq and **(H'')** anti-H3K4Me3 normalized reads at non-
1001 pioneered TFAP2-inhibited promoters. P-values shown were determined by Students
1002 t-test. **(I-L) H**ypergeometric analysis of TFAP2 regulated enhancers at TFAP2-
1003 activated (*) and TFAP2-inhibited (**) genes in *TFAP2*-KO cells (FDR < 0.05,
1004 |log2FC| > 1). The number of promoters in each category of TFAP2-regulated
1005 promoters is shown.
1006
1007 **Figure S7: Additional examples of TFAP2-activated and -inhibited promoters.**
1008 **(A-B)** Screenshots of IGV genome browser (GRCH37/hg19) visualizing anti-
1009 TFAP2A, anti-H3K4Me3, anti-H3K27Ac CUT&RUN-seq, ATAC-seq and RNA-seq
1010 profiles at **(A)** the TFAP2-activated *ZNF540* promoter and **(B)** the TFAP2-inhibited
1011 *S100A16* promoter. Genotypes as labeled; y-axes are grouped scaled per dataset.
1012
1013 **Figure S8: TFAP2 paralogs modulate the binding of MITF. (A)** Density heatmap
1014 centred on 9,413 peaks co-bound by TFAP2A and MITF, showing anti-TFAP2, anti-
1015 MITF, ATAC-seq, and anti-H3K27Ac CUT&RUN profiles in SK-MEL-28 cells.
1016 Regions shown are +/- 5 kb from peak center. **(B)** Violin plot showing anti-MITF

1017 CUT&RUN signal (RPKM) in *TFAP2*-KO and SK-MEL-28 cells at loci not bound by
1018 TFAP2A. ns; non-significant by Students t-test. **(C)** Scatterplot of TFAP2-dependent
1019 MITF peaks showing log2 normalized reads on the x-axis and log2FC on the y-axis
1020 in *TFAP2*-KO versus WT cells. **(D)** Screenshots of IGV genome browser
1021 (GRCH37/hg19); genotypes as labeled, visualizing anti-TFAP2A and anti-MITF
1022 CUT&RUN-seq and ATAC-seq profiles at TFAP2-dependent MITF peaks, mutually
1023 dependent MITF/TFAP2 peaks and an example of a non-overlapping, TFAP2-
1024 independent MITF peak. **(E)** Volcano plot showing increased H3K27Me3 CUT&RUN
1025 signal at mutually dependent TFAP2/MITF peaks in *MITF*-KO cells versus WT cells.
1026 P-values were determined by Students t-test. Normalized reads (RPKM), **(F-G)**
1027 Screenshots of IGV genome browser (GRCH37/hg19), visualizing anti-H3K27Me3
1028 CUT&RUN-seq profiles in *MIT*F-KO and WT cells. Peaks were called using MACS2
1029 software (two independent replicates) and are illustrated by blue bars. Two examples
1030 loci of mutually dependent TFAP2/MITF peaks showing increased H3K27Me3
1031 signals are shown, **(F)** at the *TRPM1* promoter and **(G)** at two *FRMD4B* enhancers.
1032 Mutually-dependent peaks are indicated by red arrows.
1033
1034 **Figure S9: Density heatmap of TFAP2 regulated MITF peaks.** Density heatmap
1035 centred on TFAP2 regulated MITF peaks (Top cluster) TFAP2-dependent MITF
1036 peaks, (Second cluster) Mutually dependent TFAP2/MITF peaks, (third cluster)
1037 TFAP2-inhibited MITF peaks and (forth cluster) independent peaks, showing two
1038 replicates of anti-MITF CUT&RUN in SK-MEL-28 and *TFAP2*-KO cells, and two
1039 replicates of anti-TFAP2A CUT&RUN in SK-MEL-28 and *MITF*-KO cells. Regions
1040 shown are +/- 5 kb from peak center.
1041
1042 **Figure S10: TFAP2 and MITF do not co-inhibit enhancers at TFAP2-inhibited or**
1043 **MITF-inhibited genes in SK-MEL-28 cells. (A-A')** Violin plot of TFAP2 dependent
1044 MITF peaks at TFAP2-inhibied enhancers (i.e. co-inhibited enhancers) showing **(B)**
1045 anti-MITF CUT&RUN and **(A')** ATAC-Seq profiles in *TFAP2*-KO and WT SK-MEL-28
1046 cells. Such loci were not significantly enriched at MITF-inhibited or TFAP2-inhibited
1047 genes. (A'') Schematic of TFAP2/ MITF co-inhibited enhancers. In this example
1048 TFAP2 is a pioneer factor recruiting MITF, in its repressor form, to condense
1049 chromatin. Loss of TFAP2 in TFAP2-KO cells results in loss of MITF-repressor
1050 binding and opening of chromatin by an alternative pioneer factor. **(B-B')** Violin plot

1051 of TFAP2-inhibited MITF peaks at modestly TFAP2-inhibted enhancers showing **(C)**
1052 anti-MITF CUT&RUN **(B')** ATAC-Seq profiles in *TFAP2*-KO and WT SK-MEL-28
1053 cells. Such loci were not significantly enriched at MITF-inhibited or TFAP2-inhibited
1054 genes. (B'') Schematic of TFAP2-inhibted MITF peaks at modestly inhibited
1055 enhancers (Log2FC > -0.5 – -1). In this example TFAP2 recruits a repressor protein
1056 and inhibits MITF binding in WT cells. In the absence of TFAP2, MITF recruits
1057 SWI/SNF and opens chromatin via an alternative pioneer factor.
1058
1059 **Figure S11: Genes that harbor TFAP2-independent anti-MITF peaks are**
1060 **enriched for cell cycle and DNA-repair. (A)** Plot-profile showing MITF CUT&RUN
1061 peak signal at TFAP2-independent MITF peaks in *TFAP2*-KO and WT SK-MEL-28
1062 cell lines. **(B)** Genes that harbor TFAP2-independent anti-MITF peaks were analyzed
1063 for enriched gene ontology biological process using GREAT (single nearest gene +/-
1064 100kb).
1065
1066 **Figure S12: Example of an TFAP2-dependent enhancer at intron 2 of MITF.**
1067 Screenshot of IGV genome browser (GRCH37/hg19) visualizing anti-TFAP2A,
1068 ATAC-seq, anti-H3K27Ac and RNA-seq profiles at intron 2 of MITF. Dashed
1069 rectangle indicates an TFAP2-dependent NDR. MITF and downstream regions are
1070 shown, blue arrows indicate strand orientation and horizontal rectangles the exons.
1071 Genotypes are as labeled; y-axes are grouped scaled per dataset.
1072
1073 **Figure S13: TFAP2 directly activates genes associated with cell differentiation**
1074 **and proliferation, and direct inhibits genes associated with cell adhesion and**
1075 **cell migration. (A-B)** The top 55 genes that are directly TFAP2-activated and
1076 associated with the GO terms **(A)** cell differentiation and pigmentation and **(B)**
1077 proliferation are represented by heatmap (log2FC). **(C)** the top 55 genes that are
1078 directly TFAP2-inhibited and associated with the GO terms cell adhesion and cell
1079 migration are represented by heatmap (log2FC). C1: *TFAP2*-KO clone 4.3, C2:
1080 *TFAP2*-KO clone 2.12. **(D)** Wound healing scratch-recovery-assay over 24 hours in
1081 WT and *TFAP2*-KO cells. *TFAP2*-KO cells show reduced migration capacity
1082 compared to wild type SK-MEL-28 cells.
1083
1084

1085 **References cited:**

1086


1087 Aras, S., Saladi, S.V., Basuroy, T., Marathe, H.G., Lores, P., de la Serna, I.L., 2019. BAF60A
1088 mediates interactions between the microphthalmia-associated transcription factor and the
1089 BRG1-containing SWI/SNF complex during melanocyte differentiation. J Cell Physiol 234,
1090 11780-11791.
1091 Atchison, M.L., 2014. Function of YY1 in Long-Distance DNA Interactions. Front Immunol
1092 5, 45.
1093 Bamforth, S.D., Braganca, J., Eloranta, J.J., Murdoch, J.N., Marques, F.I., Kranc, K.R.,
1094 Farza, H., Henderson, D.J., Hurst, H.C., Bhattacharya, S., 2001. Cardiac malformations,
1095 adrenal agenesis, neural crest defects and exencephaly in mice lacking Cited2, a new Tfap2
1096 co-activator. Nat Genet 29, 469-474.
1097 Barrallo-Gimeno, A., Holzschuh, J., Driever, W., Knapik, E.W., 2004. Neural crest survival
1098 and differentiation in zebrafish depends on mont blanc/tfap2a gene function. Development
1099 131, 1463-1477.
1100 Baxter, L.L., Loftus, S.K., Pavan, W.J., 2009. Networks and pathways in pigmentation,
1101 health, and disease. Wiley Interdiscip Rev Syst Biol Med 1, 359-371.
1102 Baxter, L.L., Watkins-Chow, D.E., Pavan, W.J., Loftus, S.K., 2019. A curated gene list for
1103 expanding the horizons of pigmentation biology. Pigment Cell Melanoma Res 32, 348-358.
1104 Bejjani, F., Evanno, E., Zibara, K., Piechaczyk, M., Jariel-Encontre, I., 2019. The AP-1
1105 transcriptional complex: Local switch or remote command? Biochim Biophys Acta Rev
1106 Cancer 1872, 11-23.
1107 Betancur, P., Bronner-Fraser, M., Sauka-Spengler, T., 2010. Assembling neural crest
1108 regulatory circuits into a gene regulatory network. Annu Rev Cell Dev Biol 26, 581-603.
1109 Braganca, J., Eloranta, J.J., Bamforth, S.D., Ibbitt, J.C., Hurst, H.C., Bhattacharya, S., 2003.
1110 Physical and functional interactions among AP-2 transcription factors, p300/CREB-binding
1111 protein, and CITED2. The Journal of biological chemistry 278, 16021-16029.
1112 Brewer, S., Jiang, X., Donaldson, S., Williams, T., Sucov, H.M., 2002. Requirement for AP-
1113 2alpha in cardiac outflow tract morphogenesis. Mech Dev 110, 139-149.
1114 Buenrostro, J.D., Giresi, P.G., Zaba, L.C., Chang, H.Y., Greenleaf, W.J., 2013. Transposition
1115 of native chromatin for fast and sensitive epigenomic profiling of open chromatin, DNA-
1116 binding proteins and nucleosome position. Nat Methods 10, 1213-1218.
1117 Buenrostro, J.D., Wu, B., Chang, H.Y., Greenleaf, W.J., 2015. ATAC-seq: A Method for
1118 Assaying Chromatin Accessibility Genome-Wide. Curr Protoc Mol Biol 109, 21.29.21-
1119 21.29.29.
1120 Campbell, N.R., Rao, A., Zhang, M., Baron, M., Heilmann, S., Deforet, M., Kenny, C.,
1121 Ferretti, L., Huang, T.-H., Garg, M., Nsengimana, J., Montal, E., Tagore, M., Hunter, M.,
1122 Newton-Bishop, J., Middleton, M.R., Corrie, P., Adams, D.J., Rabbie, R., Levesque, M.P.,
1123 Cornell, R.A., Yanai, I., Xavier, J.B., White, R.M., 2021. Cell state diversity promotes
1124 metastasis through heterotypic cluster formation in melanoma. Developmental Cell,
1125 2020.2008.2024.265140.
1126 Carreira, S., Goodall, J., Denat, L., Rodriguez, M., Nuciforo, P., Hoek, K.S., Testori, A.,
1127 Larue, L., Goding, C.R., 2006. Mitf regulation of Dia1 controls melanoma proliferation and
1128 invasiveness. Genes Dev 20, 3426-3439.
1129 Creyghton, M.P., Cheng, A.W., Welstead, G.G., Kooistra, T., Carey, B.W., Steine, E.J.,
1130 Hanna, J., Lodato, M.A., Frampton, G.M., Sharp, P.A., Boyer, L.A., Young, R.A., Jaenisch,
1131 R., 2010. Histone H3K27ac separates active from poised enhancers and predicts
1132 developmental state. Proc Natl Acad Sci U S A 107, 21931-21936.

1133 de la Serna, I.L., Ohkawa, Y., Higashi, C., Dutta, C., Osias, J., Kommajosyula, N.,
1134 Tachibana, T., Imbalzano, A.N., 2006. The microphthalmia-associated transcription factor
1135 requires SWI/SNF enzymes to activate melanocyte-specific genes. J Biol Chem 281, 20233-
1136 20241.
1137 Dilshat, R., Fock, V., Kenny, C., Gerritsen, I., Lasseur, R.M.J., Travnickova, J., Eichhoff,
1138 O.M., Cerny, P., Moller, K., Sigurbjornsdottir, S., Kirty, K., Einarsdottir, B.O., Cheng, P.F.,
1139 Levesque, M., Cornell, R.A., Patton, E.E., Larue, L., de Tayrac, M., Magnusdottir, E., Helga
1140 Ogmundsdottir, M., Steingrimsson, E., 2021. MITF reprograms the extracellular matrix and
1141 focal adhesion in melanoma. Elife 10.
1142 Dobin, A., Davis, C.A., Schlesinger, F., Drenkow, J., Zaleski, C., Jha, S., Batut, P., Chaisson,
1143 M., Gingeras, T.R., 2013. STAR: ultrafast universal RNA-seq aligner. Bioinformatics 29, 15-
1144 21.
1145 Du, J., Li, L., Ou, Z., Kong, C., Zhang, Y., Dong, Z., Zhu, S., Jiang, H., Shao, Z., Huang, B.,
1146 Lu, J., 2012. FOXC1, a target of polycomb, inhibits metastasis of breast cancer cells. Breast
1147 Cancer Res Treat 131, 65-73.
1148 Eckert, D., Buhl, S., Weber, S., Jager, R., Schorle, H., 2005. The AP-2 family of transcription
1149 factors. Genome Biol 6, 246.
1150 Fernandez Garcia, M., Moore, C.D., Schulz, K.N., Alberto, O., Donague, G., Harrison, M.M.,
1151 Zhu, H., Zaret, K.S., 2019. Structural Features of Transcription Factors Associating with
1152 Nucleosome Binding. Mol Cell 75, 921-932 e926.
1153 Goding, C.R., 2000. Mitf from neural crest to melanoma: signal transduction and
1154 transcription in the melanocyte lineage. Genes Dev 14, 1712-1728.
1155 Grossman, S.R., Engreitz, J., Ray, J.P., Nguyen, T.H., Hacohen, N., Lander, E.S., 2018.
1156 Positional specificity of different transcription factor classes within enhancers. Proc Natl
1157 Acad Sci U S A 115, E7222-E7230.
1158 Hartman, M.L., Czyz, M., 2015. MITF in melanoma: mechanisms behind its expression and
1159 activity. Cell Mol Life Sci 72, 1249-1260.
1160 Higdon, C.W., Mitra, R.D., Johnson, S.L., 2013. Gene expression analysis of zebrafish
1161 melanocytes, iridophores, and retinal pigmented epithelium reveals indicators of biological
1162 function and developmental origin. PLoS One 8, e67801.
1163 Hoek, K.S., Eichhoff, O.M., Schlegel, N.C., Döbbeling, U., Kobert, N., Schaerer, L., Hemmi,
1164 S., Dummer, R., 2008a. In vivo switching of human melanoma cells between proliferative
1165 and invasive states. Cancer Res 68, 650-656.
1166 Hoek, K.S., Schlegel, N.C., Brafford, P., Sucker, A., Ugurel, S., Kumar, R., Weber, B.L.,
1167 Nathanson, K.L., Phillips, D.J., Herlyn, M., Schadendorf, D., Dummer, R., 2006. Metastatic
1168 potential of melanomas defined by specific gene expression profiles with no BRAF signature.
1169 Pigment Cell Res 19, 290-302.
1170 Hoek, K.S., Schlegel, N.C., Eichhoff, O.M., Widmer, D.S., Praetorius, C., Einarsson, S.O.,
1171 Valgeirsdottir, S., Bergsteinsdottir, K., Schepsky, A., Dummer, R., Steingrimsson, E., 2008b.
1172 Novel MITF targets identified using a two-step DNA microarray strategy. Pigment Cell
1173 Melanoma Res 21, 665-676.
1174 Huang, S., Jean, D., Luca, M., Tainsky, M.A., Bar-Eli, M., 1998. Loss of AP-2 results in
1175 downregulation of c-KIT and enhancement of melanoma tumorigenicity and metastasis.
1176 EMBO J 17, 4358-4369.
1177 Jonsson, G., Busch, C., Knappskog, S., Geisler, J., Miletic, H., Ringner, M., Lillehaug, J.R.,
1178 Borg, A., Lonning, P.E., 2010. Gene expression profiling-based identification of molecular
1179 subtypes in stage IV melanomas with different clinical outcome. Clin Cancer Res 16, 3356-
1180 3367.

1181 Keenen, B., Qi, H., Saladi, S.V., Yeung, M., de la Serna, I.L., 2010. Heterogeneous
1182 SWI/SNF chromatin remodeling complexes promote expression of microphthalmia-
1183 associated transcription factor target genes in melanoma. Oncogene 29, 81-92.
1184 Kim, S., Yu, N.K., Kaang, B.K., 2015. CTCF as a multifunctional protein in genome
1185 regulation and gene expression. Exp Mol Med 47, e166.
1186 Knight, R.D., Javidan, Y., Nelson, S., Zhang, T., Schilling, T., 2004. Skeletal and pigment
1187 cell defects in the lockjaw mutant reveal multiple roles for zebrafish tfap2a in neural crest
1188 development. Dev Dyn 229, 87-98.
1189 Knight, R.D., Nair, S., Nelson, S.S., Afshar, A., Javidan, Y., Geisler, R., Rauch, G.J.,
1190 Schilling, T.F., 2003. lockjaw encodes a zebrafish tfap2a required for early neural crest
1191 development. Development 130, 5755-5768.
1192 Kołat, D., Kałuzińska, Ż., Bednarek, A.K., Płuciennik, E., 2021. WWOX Loses the Ability to
1193 Regulate Oncogenic AP-2γ and Synergizes with Tumor Suppressor AP-2α in High-Grade
1194 Bladder Cancer. Cancers (Basel) 13.
1195 Kuckenberg, P., Kubaczka, C., Schorle, H., 2012. The role of transcription factor
1196 Tcfap2c/TFAP2C in trophectoderm development. Reprod Biomed Online 25, 12-20.
1197 Lang, D., Lu, M.M., Huang, L., Engleka, K.A., Zhang, M., Chu, E.Y., Lipner, S., Skoultchi,
1198 A., Millar, S.E., Epstein, J.A., 2005. Pax3 functions at a nodal point in melanocyte stem cell
1199 differentiation. Nature 433, 884-887.
1200 Langmead, B., Salzberg, S.L., 2012. Fast gapped-read alignment with Bowtie 2. Nat Methods
1201 9, 357-359.
1202 Langmead, B., Trapnell, C., Pop, M., Salzberg, S.L., 2009. Ultrafast and memory-efficient
1203 alignment of short DNA sequences to the human genome. Genome Biol 10, R25.
1204 Laurette, P., Strub, T., Koludrovic, D., Keime, C., Le Gras, S., Seberg, H., Van Otterloo, E.,
1205 Imrichova, H., Siddaway, R., Aerts, S., Cornell, R.A., Mengus, G., Davidson, I., 2015.
1206 Transcription factor MITF and remodeller BRG1 define chromatin organisation at regulatory
1207 elements in melanoma cells. Elife 4.
1208 Lee, B.K., Uprety, N., Jang, Y.J., Tucker, S.K., Rhee, C., LeBlanc, L., Beck, S., Kim, J.,
1209 2018. Fosl1 overexpression directly activates trophoblast-specific gene expression programs
1210 in embryonic stem cells. Stem Cell Res 26, 95-102.
1211 Leroy, B., Girard, L., Hollestelle, A., Minna, J.D., Gazdar, A.F., Soussi, T., 2014. Analysis of
1212 TP53 mutation status in human cancer cell lines: a reassessment. Hum Mutat 35, 756-765.
1213 Li, L., Wang, Y., Torkelson, J.L., Shankar, G., Pattison, J.M., Zhen, H.H., Fang, F., Duren,
1214 Z., Xin, J., Gaddam, S., Melo, S.P., Piekos, S.N., Li, J., Liaw, E.J., Chen, L., Li, R., Wernig,
1215 M., Wong, W.H., Chang, H.Y., Oro, A.E., 2019. TFAP2C- and p63-Dependent Networks
1216 Sequentially Rearrange Chromatin Landscapes to Drive Human Epidermal Lineage
1217 Commitment. Cell Stem Cell 24, 271-284 e278.
1218 Li, W., Cornell, R.A., 2007. Redundant activities of Tfap2a and Tfap2c are required for
1219 neural crest induction and development of other non-neural ectoderm derivatives in zebrafish
1220 embryos. Dev Biol 304, 338-354.
1221 Lin, C.Y., Chao, A., Wang, T.H., Lee, L.Y., Yang, L.Y., Tsai, C.L., Wang, H.S., Lai, C.H.,
1222 2016. Nucleophosmin/B23 is a negative regulator of estrogen receptor alpha expression via
1223 AP2gamma in endometrial cancer cells. Oncotarget 7, 60038-60052.
1224 Liu, H., Duncan, K., Helverson, A., Kumari, P., Mumm, C., Xiao, Y., Carlson, J.C.,
1225 Darbellay, F., Visel, A., Leslie, E., Breheny, P., Erives, A.J., Cornell, R.A., 2020. Analysis of
1226 zebrafish periderm enhancers facilitates identification of a regulatory variant near human
1227 KRT8/18. Elife 9.
1228 Liu, H., Tan, B.C., Tseng, K.H., Chuang, C.P., Yeh, C.W., Chen, K.D., Lee, S.C., Yung,
1229 B.Y., 2007. Nucleophosmin acts as a novel AP2alpha-binding transcriptional corepressor
1230 during cell differentiation. EMBO Rep 8, 394-400.

1231 Love, M.I., Huber, W., Anders, S., 2014. Moderated estimation of fold change and dispersion
1232 for RNA-seq data with DESeq2. Genome Biol 15, 550.
1233 Luo, T., Matsuo-Takasaki, M., Thomas, M.L., Weeks, D.L., Sargent, T.D., 2002.
1234 Transcription factor AP-2 is an essential and direct regulator of epidermal development in
1235 Xenopus. Dev Biol 245, 136-144.
1236 Mavrothalassitis, G., Ghysdael, J., 2000. Proteins of the ETS family with transcriptional
1237 repressor activity. Oncogene 19, 6524-6532.
1238 Mayran, A., Khetchoumian, K., Hariri, F., Pastinen, T., Gauthier, Y., Balsalobre, A., Drouin,
1239 J., 2018. Pioneer factor Pax7 deploys a stable enhancer repertoire for specification of cell
1240 fate. Nat Genet 50, 259-269.
1241 McLean, C.Y., Bristor, D., Hiller, M., Clarke, S.L., Schaar, B.T., Lowe, C.B., Wenger, A.M.,
1242 Bejerano, G., 2010. GREAT improves functional interpretation of cis-regulatory regions. Nat
1243 Biotechnol 28, 495-501.
1244 Meers, M.P., Bryson, T.D., Henikoff, J.G., Henikoff, S., 2019. Improved CUT&RUN
1245 chromatin profiling tools. Elife 8.
1246 Mi, H., Ebert, D., Muruganujan, A., Mills, C., Albou, L.P., Mushayamaha, T., Thomas, P.D.,
1247 2021. PANTHER version 16: a revised family classification, tree-based classification tool,
1248 enhancer regions and extensive API. Nucleic Acids Res 49, D394-d403.
1249 Miller, J.C., Holmes, M.C., Wang, J., Guschin, D.Y., Lee, Y.L., Rupniewski, I., Beausejour,
1250 C.M., Waite, A.J., Wang, N.S., Kim, K.A., Gregory, P.D., Pabo, C.O., Rebar, E.J., 2007. An
1251 improved zinc-finger nuclease architecture for highly specific genome editing. Nat
1252 Biotechnol 25, 778-785.
1253 Mitchell, P.J., Timmons, P.M., Hebert, J.M., Rigby, P.W., Tjian, R., 1991. Transcription
1254 factor AP-2 is expressed in neural crest cell lineages during mouse embryogenesis. Genes
1255 Dev 5, 105-119.
1256 Mollaaghababa, R., Pavan, W.J., 2003. The importance of having your SOX on: role of
1257 SOX10 in the development of neural crest-derived melanocytes and glia. Oncogene 22, 3024-
1258 3034.
1259 Moser, M., Ruschoff, J., Buettner, R., 1997. Comparative analysis of AP-2 alpha and AP-2
1260 beta gene expression during murine embryogenesis. Developmental Dynamics 208, 115-124.
1261 Pastor, W.A., Liu, W., Chen, D., Ho, J., Kim, R., Hunt, T.J., Lukianchikov, A., Liu, X., Polo,
1262 J.M., Jacobsen, S.E., Clark, A.T., 2018. TFAP2C regulates transcription in human naive
1263 pluripotency by opening enhancers. Nat Cell Biol 20, 553-564.
1264 Pekowska, A., Benoukraf, T., Zacarias-Cabeza, J., Belhocine, M., Koch, F., Holota, H.,
1265 Imbert, J., Andrau, J.C., Ferrier, P., Spicuglia, S., 2011. H3K4 tri-methylation provides an
1266 epigenetic signature of active enhancers. EMBO J 30, 4198-4210.
1267 Petruk, S., Cai, J., Sussman, R., Sun, G., Kovermann, S.K., Mariani, S.A., Calabretta, B.,
1268 McMahon, S.B., Brock, H.W., Iacovitti, L., Mazo, A., 2017. Delayed Accumulation of
1269 H3K27me3 on Nascent DNA Is Essential for Recruitment of Transcription Factors at Early
1270 Stages of Stem Cell Differentiation. Mol Cell 66, 247-257 e245.
1271 Pihlajamaa, P., Sahu, B., Lyly, L., Aittomaki, V., Hautaniemi, S., Janne, O.A., 2014. Tissue-
1272 specific pioneer factors associate with androgen receptor cistromes and transcription
1273 programs. EMBO J 33, 312-326.
1274 Praetorius, C., Grill, C., Stacey, S.N., Metcalf, A.M., Gorkin, D.U., Robinson, K.C., Van
1275 Otterloo, E., Kim, R.S., Bergsteinsdottir, K., Ogmundsdottir, M.H., Magnusdottir, E., Mishra,
1276 P.J., Davis, S.R., Guo, T., Zaidi, M.R., Helgason, A.S., Sigurdsson, M.I., Meltzer, P.S.,
1277 Merlino, G., Petit, V., Larue, L., Loftus, S.K., Adams, D.R., Sobhiafshar, U., Emre, N.C.,
1278 Pavan, W.J., Cornell, R., Smith, A.G., McCallion, A.S., Fisher, D.E., Stefansson, K., Sturm,
1279 R.A., Steingrimsson, E., 2013. A polymorphism in IRF4 affects human pigmentation through
1280 a tyrosinase-dependent MITF/TFAP2A pathway. Cell 155, 1022-1033.

1281 Rambow, F., Job, B., Petit, V., Gesbert, F., Delmas, V., Seberg, H., Meurice, G., Van
1282 Otterloo, E., Dessen, P., Robert, C., Gautheret, D., Cornell, R.A., Sarasin, A., Larue, L.,
1283 2015. New Functional Signatures for Understanding Melanoma Biology from Tumor Cell
1284 Lineage-Specific Analysis. Cell Rep 13, 840-853.
1285 Rambow, F., Marine, J.C., Goding, C.R., 2019. Melanoma plasticity and phenotypic
1286 diversity: therapeutic barriers and opportunities. Genes Dev 33, 1295-1318.
1287 Rambow, F., Rogiers, A., Marin-Bejar, O., Aibar, S., Femel, J., Dewaele, M., Karras, P.,
1288 Brown, D., Chang, Y.H., Debiec-Rychter, M., Adriaens, C., Radaelli, E., Wolter, P., Bechter,
1289 O., Dummer, R., Levesque, M., Piris, A., Frederick, D.T., Boland, G., Flaherty, K.T., van den
1290 Oord, J., Voet, T., Aerts, S., Lund, A.W., Marine, J.C., 2018. Toward Minimal Residual
1291 Disease-Directed Therapy in Melanoma. Cell 174, 843-855 e819.
1292 Ramírez, F., Ryan, D.P., Grüning, B., Bhardwaj, V., Kilpert, F., Richter, A.S., Heyne, S.,
1293 Dündar, F., Manke, T., 2016. deepTools2: a next generation web server for deep-sequencing
1294 data analysis. Nucleic Acids Res 44, W160-165.
1295 Ringrose, L., Paro, R., 2004. Epigenetic regulation of cellular memory by the Polycomb and
1296 Trithorax group proteins. Annu Rev Genet 38, 413-443.
1297 Ross-Innes, C.S., Stark, R., Teschendorff, A.E., Holmes, K.A., Ali, H.R., Dunning, M.J.,
1298 Brown, G.D., Gojis, O., Ellis, I.O., Green, A.R., Ali, S., Chin, S.F., Palmieri, C., Caldas, C.,
1299 Carroll, J.S., 2012. Differential oestrogen receptor binding is associated with clinical
1300 outcome in breast cancer. Nature 481, 389-393.
1301 Sander, J.D., Dahlborg, E.J., Goodwin, M.J., Cade, L., Zhang, F., Cifuentes, D., Curtin, S.J.,
1302 Blackburn, J.S., Thibodeau-Beganny, S., Qi, Y., Pierick, C.J., Hoffman, E., Maeder, M.L.,
1303 Khayter, C., Reyon, D., Dobbs, D., Langenau, D.M., Stupar, R.M., Giraldez, A.J., Voytas,
1304 D.F., Peterson, R.T., Yeh, J.R., Joung, J.K., 2011. Selection-free zinc-finger-nuclease
1305 engineering by context-dependent assembly (CoDA). Nat Methods 8, 67-69.
1306 Sander, J.D., Maeder, M.L., Reyon, D., Voytas, D.F., Joung, J.K., Dobbs, D., 2010. ZiFiT
1307 (Zinc Finger Targeter): an updated zinc finger engineering tool. Nucleic Acids Res 38,
1308 W462-468.
1309 Schorle, H., Meier, P., Buchert, M., Jaenisch, R., Mitchell, P.J., 1996. Transcription factor
1310 AP-2 essential for cranial closure and craniofacial development. Nature 381, 235-238.
1311 Seberg, H.E., Van Otterloo, E., Cornell, R.A., 2017a. Beyond MITF: Multiple transcription
1312 factors directly regulate the cellular phenotype in melanocytes and melanoma. Pigment Cell
1313 Melanoma Res 30, 454-466.
1314 Seberg, H.E., Van Otterloo, E., Loftus, S.K., Liu, H., Bonde, G., Sompallae, R., Gildea, D.E.,
1315 Santana, J.F., Manak, J.R., Pavan, W.J., Williams, T., Cornell, R.A., 2017b. TFAP2 paralogs
1316 regulate melanocyte differentiation in parallel with MITF. PLoS Genet 13, e1006636.
1317 Sekiya, T., Zaret, K.S., 2007. Repression by Groucho/TLE/Grg proteins: genomic site
1318 recruitment generates compacted chromatin in vitro and impairs activator binding in vivo.
1319 Mol Cell 28, 291-303.
1320 Sherwood, R.I., Hashimoto, T., O'Donnell, C.W., Lewis, S., Barkal, A.A., van Hoff, J.P.,
1321 Karun, V., Jaakkola, T., Gifford, D.K., 2014. Discovery of directional and nondirectional
1322 pioneer transcription factors by modeling DNase profile magnitude and shape. Nat
1323 Biotechnol 32, 171-178.
1324 Skene, P.J., Henikoff, S., 2017. An efficient targeted nuclease strategy for high-resolution
1325 mapping of DNA binding sites. Elife 6.
1326 Strub, T., Giuliano, S., Ye, T., Bonet, C., Keime, C., Kobi, D., Le Gras, S., Cormont, M.,
1327 Ballotti, R., Bertolotto, C., Davidson, I., 2011. Essential role of microphthalmia transcription
1328 factor for DNA replication, mitosis and genomic stability in melanoma. Oncogene 30, 2319-
1329 2332.

1330 Swinstead, E.E., Miranda, T.B., Paakinaho, V., Baek, S., Goldstein, I., Hawkins, M.,
1331 Karpova, T.S., Ball, D., Mazza, D., Lavis, L.D., Grimm, J.B., Morisaki, T., Grontved, L.,
1332 Presman, D.M., Hager, G.L., 2016a. Steroid Receptors Reprogram FoxA1 Occupancy
1333 through Dynamic Chromatin Transitions. Cell 165, 593-605.
1334 Swinstead, E.E., Paakinaho, V., Presman, D.M., Hager, G.L., 2016b. Pioneer factors and
1335 ATP-dependent chromatin remodeling factors interact dynamically: A new perspective:
1336 Multiple transcription factors can effect chromatin pioneer functions through dynamic
1337 interactions with ATP-dependent chromatin remodeling factors. Bioessays 38, 1150-1157.
1338 Tan, C.C., Sindhu, K.V., Li, S., Nishio, H., Stoller, J.Z., Oishi, K., Puttreddy, S., Lee, T.J.,
1339 Epstein, J.A., Walsh, M.J., Gelb, B.D., 2008. Transcription factor Ap2delta associates with
1340 Ash2l and ALR, a trithorax family histone methyltransferase, to activate Hoxc8 transcription.
1341 Proc Natl Acad Sci U S A 105, 7472-7477.
1342 Tan, S.K., Lin, Z.H., Chang, C.W., Varang, V., Chng, K.R., Pan, Y.F., Yong, E.L., Sung,
1343 W.K., Cheung, E., 2011. AP-2gamma regulates oestrogen receptor-mediated long-range
1344 chromatin interaction and gene transcription. EMBO J 30, 2569-2581.
1345 Tirosh, I., Izar, B., Prakadan, S.M., Wadsworth, M.H., 2nd, Treacy, D., Trombetta, J.J.,
1346 Rotem, A., Rodman, C., Lian, C., Murphy, G., Fallahi-Sichani, M., Dutton-Regester, K., Lin,
1347 J.R., Cohen, O., Shah, P., Lu, D., Genshaft, A.S., Hughes, T.K., Ziegler, C.G., Kazer, S.W.,
1348 Gaillard, A., Kolb, K.E., Villani, A.C., Johannessen, C.M., Andreev, A.Y., Van Allen, E.M.,
1349 Bertagnolli, M., Sorger, P.K., Sullivan, R.J., Flaherty, K.T., Frederick, D.T., Jane-Valbuena,
1350 J., Yoon, C.H., Rozenblatt-Rosen, O., Shalek, A.K., Regev, A., Garraway, L.A., 2016.
1351 Dissecting the multicellular ecosystem of metastatic melanoma by single-cell RNA-seq.
1352 Science 352, 189-196.
1353 Tsoi, J., Robert, L., Paraiso, K., Galvan, C., Sheu, K.M., Lay, J., Wong, D.J.L., Atefi, M.,
1354 Shirazi, R., Wang, X., Braas, D., Grasso, C.S., Palaskas, N., Ribas, A., Graeber, T.G., 2018.
1355 Multi-stage Differentiation Defines Melanoma Subtypes with Differential Vulnerability to
1356 Drug-Induced Iron-Dependent Oxidative Stress. Cancer Cell 33, 890-904 e895.
1357 Van Otterloo, E., Li, W., Bonde, G., Day, K.M., Hsu, M.Y., Cornell, R.A., 2010.
1358 Differentiation of zebrafish melanophores depends on transcription factors AP2 alpha and
1359 AP2 epsilon. PLoS Genet 6.
1360 Van Otterloo, E., Li, W., Garnett, A., Cattell, M., Medeiros, D.M., Cornell, R.A., 2012.
1361 Novel Tfap2-mediated control of soxE expression facilitated the evolutionary emergence of
1362 the neural crest. Development 139, 720-730.
1363 Verfaillie, A., Imrichova, H., Atak, Z.K., Dewaele, M., Rambow, F., Hulselmans, G.,
1364 Christiaens, V., Svetlichnyy, D., Luciani, F., Van den Mooter, L., Claerhout, S., Fiers, M.,
1365 Journe, F., Ghanem, G.E., Herrmann, C., Halder, G., Marine, J.C., Aerts, S., 2015. Decoding
1366 the regulatory landscape of melanoma reveals TEADS as regulators of the invasive cell state.
1367 Nat Commun 6, 6683.
1368 Vierbuchen, T., Ling, E., Cowley, C.J., Couch, C.H., Wang, X., Harmin, D.A., Roberts,
1369 C.W.M., Greenberg, M.E., 2017. AP-1 Transcription Factors and the BAF Complex Mediate
1370 Signal-Dependent Enhancer Selection. Mol Cell 68, 1067-1082.e1012.
1371 Voss, T.C., Hager, G.L., 2014. Dynamic regulation of transcriptional states by chromatin and
1372 transcription factors. Nat Rev Genet 15, 69-81.
1373 Wang, X., Bolotin, D., Chu, D.H., Polak, L., Williams, T., Fuchs, E., 2006. AP-2alpha: a
1374 regulator of EGF receptor signaling and proliferation in skin epidermis. J Cell Biol 172, 409-
1375 421.
1376 Wang, X., Pasolli, H.A., Williams, T., Fuchs, E., 2008. AP-2 factors act in concert with
1377 Notch to orchestrate terminal differentiation in skin epidermis. J Cell Biol 183, 37-48.
1378 Watts, J.A., Zhang, C., Klein-Szanto, A.J., Kormish, J.D., Fu, J., Zhang, M.Q., Zaret, K.S.,
1379 2011. Study of FoxA pioneer factor at silent genes reveals Rfx-repressed enhancer at Cdx2

1380 and a potential indicator of esophageal adenocarcinoma development. PLoS Genet 7,
1381 e1002277.
1382 White, J.R., Thompson, D.T., Koch, K.E., Kiriazov, B.S., Beck, A.C., van der Heide, D.M.,
1383 Grimm, B.G., Kulak, M.V., Weigel, R.J., 2021. AP-2alpha-mediated activation of E2F and
1384 EZH2 drives melanoma metastasis. Cancer Res.
1385 Wilson, B.G., Wang, X., Shen, X., McKenna, E.S., Lemieux, M.E., Cho, Y.J., Koellhoffer,
1386 E.C., Pomeroy, S.L., Orkin, S.H., Roberts, C.W., 2010. Epigenetic antagonism between
1387 polycomb and SWI/SNF complexes during oncogenic transformation. Cancer Cell 18, 316-
1388 328.
1389 Wong, P.P., Miranda, F., Chan, K.V., Berlato, C., Hurst, H.C., Scibetta, A.G., 2012. Histone
1390 demethylase KDM5B collaborates with TFAP2C and Myc to repress the cell cycle inhibitor
1391 p21(cip) (CDKN1A). Mol Cell Biol 32, 1633-1644.
1392 Yu, G., Wang, L.G., Han, Y., He, Q.Y., 2012. clusterProfiler: an R package for comparing
1393 biological themes among gene clusters. Omics 16, 284-287.
1394 Zaret, K.S., 2020. Pioneer Transcription Factors Initiating Gene Network Changes. Annu Rev
1395 Genet 54, 367-385.
1396 Zaret, K.S., Carroll, J.S., 2011. Pioneer transcription factors: establishing competence for
1397 gene expression. Genes Dev 25, 2227-2241.
1398 Zhang, Y., Liu, T., Meyer, C.A., Eeckhoute, J., Johnson, D.S., Bernstein, B.E., Nusbaum, C.,
1399 Myers, R.M., Brown, M., Li, W., Liu, X.S., 2008. Model-based analysis of ChIP-Seq
1400 (MACS). Genome Biol 9, R137.
1401